PDE5a Inhibition Restricts Cancer Metastasis by Disrupting NPC1-Mediated Cholesterol Trafficking Through a Non-canonical cGMP-Dependent Pathway

Yarden Ariav[1], Samah Hayek[2,3], Thomas Cantore[4], Neel Sanghvi[4], Lital N Adler[1], Naama Darzi[1], Lipika R.Pal[4], David Robert Crawford[4], Tomer Malleron[2], Josh Silverbeck[2], Eliane Yardeni[7], Emma Hajaj[1,5], Efrat Ben-Zeev[6], Sanju Sinha[4], Shahar Ziman[1], Amir Shlomai[5], Sergey Malitsky[7], Maxim Itkin[7], Smadar Levin-Zaidman[7], Inna Goliand[7], Omer Goldman[1], Hila Tishler[1], Alexander Brandis[7], Tevie Mehlman[7], Yuri Kuznetsov[8], Noga Kozer[8], Karen Shamash[9], Ella Itzhaki[9], Neta Ben-Chaim Moskovits[9], Dean Ranmar[7], Salomon M. Stemmer[9], Shay Ben-Shachar[2,10], Eytan Ruppin[4,11], and Ayelet Erez[1*]

[1]Department of Molecular Cell Biology, Weizmann Institute of Science, Rehovot, Israel

[2]Clalit Research Institute, Innovation Division, Clalit Health Services, Ramat Gan, Israel

[3]Department of Epidemiology and Preventive Medicine, School of Public Health, Faculty of Medical and Health Sciences, Tel-Aviv University

[4]Cancer Data Science Lab, Center for Cancer Research, National Cancer Institute, National Institute of Health, Bethesda, MD

[5]Department of Medicine D, Beilinson Hospital, Petah Tikva, Israel

[6] Mantoux Institute for Bioinformatics, Nancy and Stephen Grand Israel National Center for Personalized Medicine (G-INCPM), Weizmann Institute of Science, Rehovot, Israel

[7]Department of Life Sciences Core Facilities, Weizmann Institute of Science, Rehovot, Israel

[8]Department of Veterinary Resources, Weizmann Institute of Science, Rehovot, Israel

[9] Felsenstein medical research center, Beilinson Hospital, Petah Tikva, Israel

[10]Faculty of Medical and Health Sciences, Tel-Aviv University; Tel Aviv, Israel

[11]Translational Research Institute and Jim and Eleanor Randall Department of Surgery, Cedars-Sinai Medical Center, Los-Angeles, CA

[*]Correspondence to: Ayelet Erez: ayelet.erez@weizmann.ac.il; Weizmann Institute of Science, P.O.Box 26, Rehovot 76100 Israel; Tel: +972-8-9343714

The authors declare no conflict of interest.

Abstract:

Non-canonical metabolic functions of signaling molecules contribute to cancer plasticity and metastatic progression. Here, we demonstrated that PDE5a inhibitors, including sildenafil (Viagra), induced lysosomal cholesterol accumulation across multiple mouse and human cancer models, reducing cholesterol bioavailability and impairing cancer cell migration and metastasis. Cancer cells exhibited heightened sensitivity due to reduced lysosomal gene expression, rendering them particularly vulnerable to disrupted cholesterol trafficking. Mechanistically, elevated cGMP bound the lysosomal cholesterol transporter NPC1, impairing cholesterol export and phenocopying Niemann–Pick type C pathology. The resulting cholesterol depletion disrupted membrane lipid rafts and mitochondrial bioenergetics, thereby limiting metastatic capacity and triggering compensatory SREBP2 activation with increased cholesterol synthesis. Combining sildenafil with statins yields additive antimetastatic effects by concurrently blocking lysosomal cholesterol export and cholesterol biosynthesis. Consistently, analysis of digital health records demonstrated significantly improved survival among sildenafil users, with a dose-dependent additive benefit observed when combined with statins. Together, these findings identify increasing cGMP levels through PDE5a inhibition as a potential strategy to restrict metastasis and offer a potential mechanistic basis for the beneficial effects of sildenafil.

Significance:

PDE5a inhibition is linked to lysosomal cholesterol trafficking and reduced metastasis via cGMP-mediated disruption of NPC1 export, providing insights into how non-oncologic drugs and host–tumor metabolism influence progression and outcomes.

Introduction

Cancer cells exhibit remarkable metabolic adaptability, enabling them to thrive and proliferate under constantly changing environmental conditions. This adaptability is partly achieved by repurposing specific metabolites as signaling molecules, while traditional signaling molecules regulate metabolic pathways.

In our previous work, we demonstrated the dual role of the arginine-aspartate cycle in cancer, showing that arginine metabolism regulates both nitric oxide (NO) signaling and aspartate availability for pyrimidine nucleotide synthesis(1,2). We additionally found that increasing pyrimidine availability relative to purines enhances the anti-tumor immune response to therapy by introducing a mutational bias that favors the generation of more hydrophobic, and therefore more immunogenic, peptides(3).

Cyclic guanosine monophosphate (cGMP) is a cyclic nucleotide derived from the purine guanosine triphosphate (GTP) that acts as a second messenger mainly for NO signaling. cGMP has been shown to activate various protein kinases, influencing both pro- and anti-tumorigenic effects depending on the cellular context(4). Sildenafil (Viagra), an FDA-approved, well-established Phosphodiesterase type 5A (PDE5a) inhibitor, increases cGMP levels by preventing its hydrolysis to GMP. PDE5a is an enzyme that hydrolyzes cGMP, thereby regulating various physiological processes. PDE5a is expressed in multiple tissues, including the reproductive system, heart, lungs, and skeletal muscle(5), with predominant localization in vascular tissues. There, it plays a key role in modulating smooth muscle relaxation and blood flow(6). Structurally, PDE5a consists of a catalytic domain responsible for its enzymatic function, along with regulatory regions that modulate its interaction with cGMP and other proteins(7). Its widespread distribution highlights its importance in both normal physiology and disease, positioning PDE5a as a critical therapeutic target in conditions such as erectile dysfunction and pulmonary hypertension, where vasodilation is a central mechanism of action.

Although sildenafil has a well-documented safety profile from widespread clinical use, its impact on cancer remains controversial, with conflicting evidence reported (medRxiv 2024.04.23.24304634)(8). We hypothesized that the conflicting outcomes of PDE5a inhibition in cancer may reflect an unrecognized, non-canonical function of cGMP(4,9), which, once elucidated, could be therapeutically exploited.

Materials and methods

Cell cultures

Cells were cultured using standard procedures in a 37 °C humidified incubator with 5% CO_2 in DMEM or RPMI (Gibco), supplemented with 10% heat-inactivated fetal bovine serum, 10% penicillin/streptomycin, 10% Sodium pyruvate, and 2 mM glutamine. The following cell lines were used in the study: MDA-MB-231 (DMEM), MCF7 (DMEM), MC38 (DMEM), HEK293 (DMEM), 3T3-L1 (DMEM), A549 (DMEM), LLC (DMEM) and KPC (DMEM), 4T1 (RPMI), HCT-116 (RPMI), and DU-145 (RPMI). MCF10A cells were grown with DMEM/F12, supplemented with 5% horse serum, 20 ng/ml EGF, 0.5 µg/ml hydrocortisone, 100 ng/ml cholera toxin, 10 µg/ml insulin, and 1% Pen/Strep. THLE-2, primary human hepatocytes were grown with BEGM BulletKit medium (Lonza #C-3171 & CC-4175), treated with 5uM of acetylcholine chloride (Sigma-Aldrich #A2661). Cell lines were obtained either directly from the American Type Culture Collection (ATCC), institutional cell repositories, or collaborating laboratories and were maintained according to the supplier's recommendations. The following cell lines were kindly provided by colleagues: MCF7 and MCF10A (Prof. Sima Lev), MC38 (Prof. Eran Elinav), 3T3-L1 (Prof. Amnon Bar-Shir), LLC (Prof. Karina Yaniv), KPC (Prof. Avigdor Scherz), and HCT116 and RPMI-8226 (Prof. Moshe Oren). The cell lines were not re-authenticated after receipt in our laboratory. All cell lines were routinely tested for mycoplasma contamination approximately once per month using the Mycoplasma EZ-PCR Test Kit (Biological Industries, #20-700-20, Kibbutz Beit Ha'emek, Israel), and all cultures were confirmed to be mycoplasma-free throughout the study. For 3D cultures, cells were grown on Corning Elplasia plates according to the manufacturer's instructions. For all experiments, cells were not used above passage 15.

Primary TNBC tumor cell experiments:

Triple-negative breast cancer (TNBC) primary tumor cells were obtained from patient-derived xenografts (PDX) mice models (RA-383B; RA-283; RA-152C) as described by Moskovits et al(10). For all assays performed using these TNBC cell lines, cells were seeded 24 hours prior to treatment to achieve 75–80% confluence at the start of the experiment.

For cholesterol quantification, TNBC cell lines were treated with 100 µM sildenafil for 24 hours. Cholesterol levels were determined using the Cholesterol/Cholesterol Ester-

Glo™ Assay (Promega), and data were normalized to the total protein concentration of the corresponding lysates. For Western blotting, TNBC cell lines were treated with 100 μM sildenafil for 24 hours and prepared for Western blotting as described above.

shRNA knockdowns

The lentiviral pLKO Mouse PDE5a shRNA Clone 1 (TRCN0000114993), Mouse PDE5a shRNA Clone 2 (TRCN0000114995), Mouse NPC1 Clone 1 (TRCN0000012123), Mouse NPC1 Clone 2 (TRCN0000012124), and shGFP control were purchased from Sigma-Aldrich. Lentiviral particles were produced in HEK293 cells. 4T1 cells were selected with puromycin (2 μg ml^{-1}).

RNA processing and quantitative PCR

RNA was extracted using the RNeasy Mini Kit (Qiagen, cat. no. 74104). Complementary DNA was synthesized from 1 μg of total RNA using the qScript cDNA Synthesis Kit (Quanta, cat. no. 95749). Quantitative PCR was performed using SYBR Green PCR Master Mix (Thermo Fisher Scientific, cat. no. 4385612) and gene-specific primers. All primers are detailed in the **Supplementary Table 1**.

RNA sequencing:

Total RNA-Seq samples were pooled and sequenced on NovaSeq 6000 S4 using Illumina® Stranded Total RNAPrep, Ligation with Ribo-Zero Plus and paired-end sequencing. Volcano plots were generated with Graph pad PRISM (RRID:SCR_002798).

Western blotting

Cells were lysed in RIPA buffer (Sigma-Aldrich) supplemented with 1% protease inhibitor cocktail (Calbiochem) and 1% phosphatase inhibitor cocktail (P5726, Sigma-Aldrich). Following centrifugation, the supernatant was collected, and protein content was evaluated using the BCA Protein Assay Kit (Thermo Fisher Scientific, Cat# 23225). A total of 10–20 μg protein from each sample under reducing conditions was loaded into each lane and separated by electrophoresis on a 10–15% SDS polyacrylamide gel. Following electrophoresis, proteins were transferred to cellulose nitrate membranes (Tamar, Jerusalem, Israel). Nonspecific binding was blocked by incubation with TBST (10 mM Tris–HCl (pH 8.0), 150 mM NaCl, 0.1% Tween-20) containing 5% skim milk or 3% BSA (Sigma-Aldrich, Cat# A7906) for 1 h at room temperature.

Membranes were subsequently incubated with primary antibodies against: GAPDH (1:5000; mouse monoclonal, Thermo Fisher Scientific, Cat# AM4300, RRID: AB_437392; or rabbit monoclonal, Cell Signaling Technology, Cat# 5174, RRID: AB_10622025), LC3B (1:1000; rabbit polyclonal, GeneTex, Cat# GTX127375, RRID: AB_11176277; or mouse monoclonal, Cell Signaling Technology, Cat# 83506, RRID: AB_2800018), SQSTM1/p62 (1:1000, rabbit monoclonal, Abcam, Cat# ab109012, RRID: AB_2810880), LSS (1:1000, Proteintech, Cat# 18693-1-AP, RRID: AB_2138608), MVK (1:1000, Proteintech, Cat# 12228-1-AP, RRID: AB_2147565), HMGCS1 (1:1000, Proteintech, Cat# 17643-1-AP, RRID: AB_2248359), LDLR (1:3000, Proteintech, Cat# 10785-1-AP, RRID: AB_2281164), PDE5a (1:2000; Cell Signaling Technology, Cat# 2395, RRID: AB_2161269; or Proteintech, Cat# 22624-1-AP, RRID: AB_2879137), NPC1 (1:1000, Proteintech, Cat# 13926-1-AP, RRID: AB_2152050), NPC2 (1:1000, Proteintech, Cat# 19888-1-AP, RRID: AB_10639363), and Phospho-VASP (Ser239) (1:1000, Cell Signaling Technology, Cat# 3114, RRID: AB_2213396).

Antibody binding was detected using horseradish peroxidase (HRP)-conjugated secondary antibodies (donkey anti-rabbit IgG, Abcam, Cat# ab97085, RRID: AB_10679957; or donkey anti-mouse IgG, Abcam, Cat# ab98799, RRID: AB_10675068) and enhanced chemiluminescence western blotting detection reagents (Radiance ECL Chemiluminescent Substrate, Azure). Gels were quantified using the Gel Doc XR+ system (Bio-Rad) and analyzed with Image Lab 5.1 software (Bio-Rad RRID:SCR_014210). The relative intensity of each band was calculated by dividing the specific band intensity by the loading control value. Western blot were repeated 2-4 times, and p-values were calculated using two-tailed Student t-tests between technical replicates.

Flow cytometry

Apoptosis experiments with Apotracker

Cells were plated and grown overnight in 6 or 24-well plates. The following day, cells were cultured with or without lipid-depleted serum (LDPS) and treated with sildenafil for the indicated durations. Cells were then washed, trypsinized, and transferred to 96-well U-bottom plates. Apoptosis was assessed by staining with Apotracker™ Green (1 μM, BioLegend) for 20 min, followed by DAPI (1:10,000, BioLegend) immediately before acquisition on a Beckman Coulter CytoFLEX flow cytometer.

Apotracker Green fluorescence was detected using the FITC channel, and DAPI using the PB-450 channel. Flow cytometry results were analyzed by Flowjo (RRID:SCR_008520).

shPDE5A BODIPY detection

shGFP- and shPDE5a-expressing cells were trypsinized and transferred into 96-well U-bottom plates. Cells were incubated with 1 μM BODIPY™ 493/503 for 20 minutes at 37°C, followed by two washes with PBS. Fluorescence was then measured using the FITC channel.

Cell viability experiments with crystal violet

Cells were seeded in 6 or 12-well plates at a density of 80,000–150,000 cells per well. After treatment with the indicated compounds, cells were washed once with PBS and fixed in 4% paraformaldehyde. Cells were then stained with 0.1% crystal violet (C0775, Sigma-Aldrich) for 20 minutes and washed three times with DDW. After imaging with the BioTek Cytation C10 Confocal Imaging Reader, cells were incubated with 10% acetic acid for 20 minutes with shaking. The extracted dye was diluted in water, and absorbance was measured at 590 nm using the Cytation C10.

Incucyte Proliferation assays

Cell proliferation was monitored using the IncuCyte system (Essen Bioscience). Cells were seeded in 96-well plates and allowed to adhere overnight. The next day, cells were washed with PBS, and the indicated compounds were added. Cells were imaged every 1.5–2 hours for 24–48 hours using a 4× objective. Growth curves were generated using IncuCyte analysis software (RRID:SCR_019874), and statistical analyses were performed in GraphPad Prism (RRID:SCR_002798).

Incucyte Migration Assays

Cell migration was monitored using the IncuCyte system. Cells (50k cells per well for 4T1, DU-145, HCT-116, A549 and LLC, 40k cells per well for MCF7 and 100k cells per well for MC38) were plated in an IncuCyte 96-Well ImageLock Plate (Sartorius, BA-04856) and incubated overnight. The next day, a scratch was created in the cell monolayer using the IncuCyte Wound Maker. Cells were washed with PBS, treated with the indicated compounds, and wound confluence was continuously monitored to quantify cell migration.

Cells were imaged at 1.5-, 2, and 4-hour intervals for 24 to 48 hours using a 4× objective. Data were analyzed using IncuCyte software (RRID:SCR_019874) to generate migration curves. Statistical analysis was performed using GraphPad Prism (RRID:SCR_002798).

Transwell assays:

4T1 cells were seeded at 50,000 cells in the upper chamber in a technical triplicate using a 24-well Transwell plate (Corning) in the absence of serum. As an attractant we used 20% serum in the lower chamber and incubated the cells for 24-hours treated with 100uM sildenafil. At the end of incubation, transwells were washed with PBS, fixed in 4% Paraformaldehyde, and then stained with 0.2% Crystal violet. The migrated cells were stained on the outer surface of the lower chamber and captured with the Cytation10. Quantification was done using ImageJ (RRID:SCR_003070).

.MCF7 LAMP1 overexpression

MCF7 cells were transduced with pLJC5-LAMP1-RFP-3×HA lentivirus, selected with puromycin, and used for downstream experiments. pLKO shGFP was used as an empty vector control.

Cholesterol rescue experiments

Depending on the assay, cells were seeded on plates and cultured overnight. The following day, cells were treated with Sildenafil and with/without Water Soluble Cholesterol (Sigma, 25uM) for the desired time.

Colony assays

The next day, cells were treated with sildenafil for 7 days. Cells were washed with PBS, fixed with 4% paraformaldehyde for 15 min, and stained with 0.2% crystal violet for 10 min. After three washes with UPW, the plates were dried overnight. Colonies were imaged using the Cytation C10 Confocal Imaging Reader, and the percentage of colony area was quantified using ImageJ (RRID:SCR_003070).

Respirometry (seahorse) assays

Oxygen consumption of intact 4T1 cells was assessed using the Seahorse Bioscience XF96 platform (Agilent Technologies, USA, RRID:SCR_026694). 4T1 cells were seeded at a density of 50,000 cells per well in a Seahorse microplate one day before the experiment. On the day of the experiment, the cells were pre-incubated for 4 hours with 100 μM Sildenafil, washed twice, and incubated with freshly prepared XF assay

medium (Seahorse XF Base Medium + 2 mM l-glutamine + 1 mM pyruvate + 10 mM glucose) for 1 h. Respiration was measured under basal conditions, followed by the addition of oligomycin (ATP synthase inhibitor, 1.5 µM; Cat# O4876, Sigma-Aldrich) and FCCP (Carbonyl cyanide 4-(trifluoromethoxy) phenylhydrazone, 0.5 µM; Cat# C2920, Sigma-Aldrich), which stimulates the electron transport chain to reveal the maximal oxygen consumption rate (OCR). Respiration was then halted by the addition of electron transport chain inhibitors rotenone (0.5 µM; Cat# R8875, Sigma-Aldrich) and antimycin A (0.5 µM; Cat# A8674, Sigma-Aldrich). OCR values were normalized to the cell count per well. Cell count was determined by staining the nuclei with cyQUANT (10 µg/mL; Cat# C35011, CyQUANT™ Direct Cell Proliferation Assay) and quantifying them using the Infinite M200PRO (TECAN) plate reader. Fluorescence intensity was measured with the Infinite M200PRO (TECAN) after excitation at 480 nm and emission at 520 nm.

Transmission electron microscopy

Sildenafil-treated 4T1 cells were fixed with 3% paraformaldehyde and 2% glutaraldehyde in 0.1 M cacodylate buffer containing 5 mM CaCl2 (pH 7.4). Then postfixed in 1% osmium tetroxide supplemented with 0.5% potassium hexacyanoferrate trihydrate and potassium dichromate in 0.1 M cacodylate (1 h), stained with 2% uranyl acetate in water (1 h), dehydrated in graded ethanol solutions and embedded in Agar 100 epoxy resin (Agar Scientific Ltd., Stansted, UK). Ultrathin sections (70–90 nm) were viewed and photographed with a FEI Tecnai SPIRIT (FEI, Eindhoven, Netherlands) transmission electron microscope operated at 120 kV and equipped with an EAGLE CCD Camera.

Histopathologic Staining Analyses:

Following cancer cell injection, PFA-fixed lung tissue was embedded in paraffin blocks. The blocks were sectioned into 4 µm, and tissue sections were backed at 37°C overnight. Hematoxylin and eosin staining was performed according to a standard protocol including the following steps: deparaffinization, rehydration, staining with hematoxylin and eosin, followed by dehydration. The slides were cleaned with xylene and mounted.

Cholesterol quantification by GC/MS

After various treatments, 4t1 cell pellets were dried, weighted and grinded to fine powder with 3.2mm stainless still bullets. The dry pellet was resuspended in 2:1 chloroform: methanol extraction buffer containing 5alpha cholesterolstane as internal standard, vortexed and incubated for 30min in 75C with a slight rotation. After 15min sonication 50% of the mixture was centrifuged at 15,000RPM at 4C for 15min and the supernatant was collected for the cholesterol fraction. The remaining of the mixture was dried under gentle nitrogen flow and saponified with 6% KOH in methanol at 90 °C for 1 hour, followed by the addition of 1ml of DDW and 1 mL Hexane (HPLC grade), vortexed and spun down for 5 minutes at 2500RPM. The upper phase was collected for the total cholesterol fraction, evaporated under nitrogen and the tubes were rewashed with chloroform to concentrate the extracts at the tubes' bottom. Cholesterol fractions were evaporated and Lyophilized. The dried samples were derivatized with 60ul N-Methyl-N-(trimethylsilyl) trifluoroacetamide for 1hr at 37 °C and subsequently analyzed on the GCMS. GC-MS analysis used a gas chromatograph (7820AN, Agilent Technologies) interfaced with a mass spectrometer (5975 Agilent Technologies). An HP-5ms capillary column 30 m × 250 µm × 0.25 µm (19091S-433, Agilent Technologies) was used. Helium carrier gas was maintained at a constant flow rate of 1.0 mL min−1. The GC column temperature was programmed from 170 to 280°C via a ramp of 37°C min−1, 280-300°C via a ramp of 1.5°C min−1 and maintained at 300°C for an additional 5 min. The MS was by electron impact ionization and operated in full-scan mode from m/z = 30-500. The inlet and MS transfer line temperatures were maintained at 280°C, and the ion source temperature was 250°C. Agilent MassHunter software v10.2 (RRID:SCR_016657) was used for acquisition and data processing. The levels of cholesterol in each batch were normalized to the internal standard and the dry weight of each sample.

Lipidomics analysis

Metabolite extraction

Extraction and analysis of lipids were performed as previously described in Malitsky *et al*.(11). Cell pellets were extracted with 1 ml of a pre-cooled (−20˚C) homogenous methanol: methyl-tert-butyl-ether (MTBE) 1:3 (v/v) mixture, containing following internal standards: 0.1 µg/ml of Phosphatidylcholine (17:0/17:0) (Avanti), 0.4 µg/ml of Phosphatidylethanolamine (17:0/17:0, 0.15 nmol/ml of Ceramide/Sphingoid Internal Standard Mixture II (Avanti, LM6005), 0.0267 µg/ml d5-TG Internal Standard Mixture

I (Avanti, LM6000) and 0.1 µg/ml Palmitic acid-13C (Sigma, 605573). The tubes were vortexed, then sonicated for 30 min in an ice-cold sonication bath (vortexed briefly every 10 min). Then, UPLC-grade water (DDW): methanol (3:1, v/v) solution (0.5 mL), was added to the tubes followed by vortex and centrifugation. The upper organic phase was transferred into a 2 ml Eppendorf tube. The polar phase was re-extracted as described above, with 0.5 ml of MTBE. Both organic phases were combined and dried under a gentle stream of nitrogen and then stored at −80˚C until analysis. For analysis, the dried lipid extracts were re-suspended in 200 µl mobile phase B (see below) and centrifuged at 20800 rcf (4˚C for 10 min). Then 150 µl were transferred to the HPLC vials for injection.

LC-MS for lipidomics analysis

Lipid extracts were analyzed using a Waters ACQUITY I class UPLC system coupled to a mass spectrometer (Thermo Q Exactive Plus Orbitrap, RRID:SCR_020556). which was operated in switching positive and negative ionization mode. The analysis was performed using the Acquity UPLC System combined with chromatographic conditions as described in Malitsky et al. (11)., with small alterations. Briefly, the chromatographic separation was performed on an ACQUITY UPLC BEH C8 column (2.1×100 mm, i.d., 1.7 µm) (Waters Corp., MA, USA). The mobile phase A consisted of DDW: Acetonitrile: Isopropanol 46:38:16 (v/v/v) with 1% 1 M NH_4Ac, 0.1% acetic acid. Mobile phase B composition is DDW: Acetonitrile: Isopropanol 1:69:30 (v/v/v) with 1% 1 M NH_4Ac, 0.1% acetic acid. The column was maintained at 40˚C, and the flow rate of the mobile phase was 0.4 ml/min. Mobile phase A was run for 1 min at 100%, then gradually reduced to 25% at 12 min, followed by a decrease to 0% at 16 min. Then, mobile phase B was run at 100% till 21 min, and mobile phase A was set to 100% at 21.5 min. Finally, the column was equilibrated at 100% A till 25 min.

LC-MS for PG vs BMP analysis

Analysis of bis(monoacylglycerol) hydrogen phosphate (BMP) and the phosphatidylglycerol (PG), was performed by injecting the same lipid extracts, which were analyzed using a Waters ACQUITY UPLC system coupled to a Vion IMS QTof mass spectrometer (Waters Corp.). The chromatographic system and MS parameters were set up as described in Gnainsky *et al(12)*.

Lipid identification and quantification

Orbitrap data was analyzed using LipidSearch™ software (Thermo Fisher Scientific, RRID:SCR_023716). The validation of the putative lipid identification was performed

by comparing it with a homemade library containing lipids produced by various organisms and by examining the correlation between retention time (RT) and carbon chain length and degree of unsaturation. Vion data was analyzed using UNIFY v1.9.4 (Waters Corp.). We initially identified ~2500 mass signals matching PG or BMP (Based on the Lipidmaps.org database). Compounds with correct putative ion mobility and observed in at least 3 biological replicates were used for further annotation. Compounds with characteristic PG fragments (Diacyl Glycerol, and often a neutral loss of glycerophosphate) and correct elution order were defined as PGs. BMPs were identified as compounds with correct elution order (matching standards) and lacking the characteristic PG fragments.

Hits with an average mass accuracy greater than 5 ppm were removed. Relative lipid levels were normalized to the internal standards and to the protein amount in the examined samples.

Plasma cGMP measurement

Plasma (50uL) was extracted with ethanol (150µL), and $^{15}N_5$-AMP (1ul, 50uM) was added. The mixture was vortexed and incubated at 10oC for 30min, then centrifuged (21,000 x g, 5 min). The supernatant was collected, concentrated in nitrogen flow to about 20uL, and water was added to get a final volume of 100uL.

Liquid chromatography and mass spectrometry

The LC-MS/MS instrument consisted of Acquity I-class UPLC system and Xevo TQ-S triple quadrupole mass spectrometer (Waters). Chromatographic separation was carried out using 20mM ammonium formate, pH 3.0 and acetonitrile as mobile phases A and B, respectively, with a flow 0.3mL/min and a gradient: from 2% to 15%B during first minute, then to 50%B for an additional 4 min, followed by washing (100%B), and back to initial conditions. Total runtime 9min. using BEH AX column 100 x 2.1-mm i.d. (Waters) and injection volume of 3uL. Mass detection was performed in electrospray positive mode ionization (2.5 kV), with the multiple-reaction monitoring parameters 346.3>110.1 (40), 346.3>135.1 (40), 346.3>152.1 (16) m/z (collision energy, V). MassLynx and TargetLynx software (v. 4.2 Waters, RRID:SCR_014271) were applied for quantitative analysis.

Lysosomal PH assay

For the lysosomal pH assay, fluorescence was measured using a plate reader following the protocol described in Ma et al*(13)*. Briefly, Cells were plated on black 96-well plates

(Greiner) prior to the measurement. After various treatments, cells were incubated with a pH-sensitive fluorescent probe (LysoSensor™ Yellow/Blue DND-160, 3 μM, Thermo Fisher), allowing real-time monitoring of lysosomal pH changes. Data were analyzed to determine luminal pH using fluorescence intensity ratios corresponding to different pH Buffers.

Cytation10 imaging

BODIPY, Lysotracker and mitosox staining

The day before imaging, cells were seeded into black 96-well plates. After the indicated treatments, cells were stained for 30 min with BODIPY™ 493/503 (1 μM, Thermo Fisher), LysoTracker™ Red DND-99 (50 nM, Thermo Fisher), and MitoSOX™ Red (100 nM, Thermo Fisher). Cells were then washed with PBS, stained with Hoechst 33342 (Thermo Scientific, #62249), and incubated in HBSS (Gibco) for live imaging. Cell and fluorescence metrics was quantified using Gen5 software (RRID:SCR_017317).

Immunofluorescence of LC3B, P62, and SREBP2

Following sildenafil treatment, cells were fixed with 4% paraformaldehyde for 15 min at room temperature, permeabilized with 0.2% Triton X-100 in PBS, and blocked with PBS containing 1% BSA and 22.52 mg/mL glycine. Cells were incubated overnight with primary antibodies: LC3B (1:200, Cell Signaling, E5Q2K-83506, RRID: AB_2800018), P62 (1:200, Abcam, EPR4844, RRID: AB_2810880), or SREBP2 (1:150, Cayman, 10007663, RRID: AB_639489). After three PBS washes, cells were incubated with secondary antibodies for 1 h, washed again, stained with Hoechst 33342 or DRAQ5, and imaged.

CTSB imaging

Following treatment, cells were stained with Cholesterolra Toxin Subunit B Alexa Fluor™ 647 conjugate (1:1000, Thermo Fisher) for 30 min, then fixed with 4% paraformaldehyde for 15 min at room temperature. After PBS washing, cells were stained with Hoechst 33342 and incubated in HBSS prior to imaging.

Plasma membrane cholesterol imaging

Following treatment, Cells were stained with the D4-EGFP probe (2 μg/mL, 30 min), fixed with 4% paraformaldehyde for 15 min, washed with PBS, stained with Hoechst 33342, and imaged.

Live cGMP Imaging

For live-cell cGMP imaging, cells were seeded into black 96-well plates and transfected with the Green cGull cGMP sensor[79] using Lipofectamine 2000 (Thermo Scientific). After 24 hours, cells were washed with HBSS and set at the Cytation10 microscope. Cells were first imaged to establish a baseline, after which HBSS containing the indicated compounds was injected directly into the wells. Imaging continued for 1 minute at 2-second intervals using a ×60 objective with GFP excitation and emission settings. To compare cGMP levels between treatment groups, X cells exhibiting green cGull fluorescence in each group were identified, and the average signal intensity was determined for each group.

2-photon and co-localization imaging with filipin

Filipin/BODIPY imaging

50,000 cells were plated on #1.5H coverslips (Marienfeld, Lauda-Königshofen, Germany), treated with the indicated compounds, and fixed 24 h later with 4% paraformaldehyde for 15 min at room temperature. Cells were stained sequentially as follows: Filipin (0.5 mg/mL; Cayman #70440) for 45 min in the dark, BODIPY™ 493/503 (2 μM, Thermo scientific) for 30 min in the dark and DRAQ5 (5 μM; Cell Signaling #4084) for 5 min in the dark Each staining step was followed by three PBS washes. Coverslips were mounted with Fluoromount-G™ (Invitrogen).

Filipin/LAMP1 co-localization

30,000 cells were plated on #1.5H coverslips, treated with sildenafil, and fixed after 24 h with 4% paraformaldehyde. Cells were permeabilized with 0.1% saponin and blocked with PBS containing 1% BSA and 22.52 mg/mL glycine. Cells were incubated overnight with primary LAMP1 antibody (1:50, DSHB, 1D4B, RRID: AB_2134500), washed, and then incubated for 1 h with Goat Anti-Rat IgG H&L (1:500, Alexa Fluor® 594, Abcam, Cat# ab150160, RRID:AB_2756445). Filipin (0.5 mg/mL) was added during the secondary antibody incubation. Coverslips were mounted for imaging.

TMEM192-GFP/Filipin co-localization

30,000 cells were plated on #1.5H coverslips and transfected with pLJM1-FLAG-GFP-TMEM192 (Addgene #134630) using Lipofectamine 2000. After 24 h, cells were treated with sildenafil and fixed with 4% paraformaldehyde 24 h later. After PBS washes, cells were stained with Filipin and DRAQ5 and mounted.

Intacellular cholesterol D4-EGFP staining

50,000 cells were seeded on coverslips and treated with sildenafil for 24h. staining and imaging was done as described by Wilhelm et al., 2019(14).

Imaging was performed using an upright Leica TCS SP8 multi-photon microscope equipped with external non-descanned HyD detectors (NDD HyD) and an acousto-optical tunable filter (Leica Microsystems CMS GmbH, Germany). For Filipin, excitation was achieved at 700 nm using a tunable femtosecond laser (Coherent Vision II, Coherent GmbH, USA), and emission was collected with an external NDD HyD detector through a 440 nm long-pass filter. BODIPY green, D4-EGFP and TMEM192-GFP were excited with a 488 nm Argon laser, with emission collected at 493–540 nm on a HyD detector. DRAQ5 was excited with a HeNe 633 nm laser, with emission collected at 643–720 nm. LAMP1–Alexa 594 was excited with a HeNe 561 nm laser, with emission collected at 604–630 nm. Images were acquired using a Galvo scanner at 1728 × 1728 pixel resolution (XY) through an HC PL APO CS2 63×/1.40 OIL objective (506350, Leica). Acquisition parameters were scanning speed 600 Hz, zoom 1, line averaging 4, 16-bit depth, Z-step 0.299 µm, and pixel size 0.101 µm (XY). Z-stacks were collected using the Galvo stage. All images were visualized using LAS X software (Leica Application Suite X, Leica Microsystems CMS GmbH, RRID:SCR_013673).

Plasma membrane cholesterol and filipin co-staining

50,000 cells were seeded on coverslips and treated with sildenafil (100 µM), lovastatin (1 µM), or both for 24 hours. Cells were washed with PBS and incubated with 5 µg/mL D4-EGFP for 30 minutes at 37 °C. After staining, cells were fixed with 4% paraformaldehyde for 15 minutes at room temperature, then stained with 0.25 mg/mL filipin for 45 minutes and Draq5 for 5 minutes before mounting on slides.

Imaging was performed using a Leica MICA microscope in confocal laser scanning mode (Leica Microsystems CMS GmbH, Germany). Cells were imaged through an HC PL APO CS2 63×/1.40 Oil UV objective. Filipin, EGFP, and DRAQ5 were excited using 405 nm, 488 nm, and 637 nm lasers, respectively. Images were acquired at a pixel

size of 93 nm using a scan speed of 600 Hz (bidirectional), line averaging of 4, a pinhole size of 1.0 Airy unit (43 µm), and a bit depth of 8. Images were visualized using LAS X software (Leica Application Suite X, version 6.2.4.29609; Leica Microsystems CMS GmbH). Fluorescent images were analyzed for the Filipin marker using QuPath v0.6 (https://qupath.readthedocs.io/en/stable/index.html). Analysis methodology included the following steps: i. Segmentation using Cellpose-3 , using the 'nuc' pre-trained model (https://github.com/MouseLand/cellpose, https://github.com/BIOP/qupath-extension-cellpose) ii. An object classifier was then trained on selected ROIs from the image set to classify the Filipin marker as positive/negative. The ROIs were selected to reflect both inter- and intra-image variability. iii. The Filipin object classifier was then applied to each image of image-set. The classification was run on the whole tissue of each image. iv. The results were then saved as a CSV file for further quantification of the number of positive/negative cells for the Filipin marker per image. v. The whole procedure (i-iv) was implemented in a short groovy script that was run on a batch of about twenty images in the QuPath (RRID:SCR_018257) script editor.

In vivo experiments

lung metastasis experiments:

6–8-week-old female BALB/cOlaHsd (RRID:IMSR_ENV:HSD-162) mice were inoculated with 4T1 cells Intravenously (2×10^5 cells). For MC38 and LLC experiments, 6–8-week-old female C57BL/6JOlaHsd (RRID:IMSR_ENV:HSD-057) mice were used to intravenously inject 1.5×10^5 cells (MC38) and 1×10^6 (LLC). Mice were sacrificed after 12-14 d (Intravenously) using ketamine–xylene or Pental. Lungs were extracted and fixed immediately in 4% paraformaldehyde. A subgroup of experimental animals received Sildenafil (Molekula group, 100 mg/kg/day in drinking water), Lovastatin (Molekula group, 10 mg/kg, days 0, 2, 4, 7 and 9 via oral gavage) or both, while the remaining mice had water without the drug, and received a control gavage. Administration of Sildenafil started 8 hours after tumor administration. For shRNA experiments, shGFP and mouse shPDE5a-1 and shNPC1-1 constructs were used. Metastatic load was calculated by dividing the lung foci with the total lung area.

Spontaneous metastases experiments:

6–8-week-old female BALB/cOlaHsd (RRID:IMSR_ENV:HSD-162) mice were inoculated with 4T1 cells in the Mammary fat pad. (0.5×10^6 cells). Mice were

sacrificed after 28 d. Tumor volumes were measured at the end of each experiment using a caliper and weighed. Lungs were extracted and immediately fixed in 4% paraformaldehyde for metastasis detection. Lung metastases were counted in each group and normalized to the mice's tumor weight.

NSG mice experiments:

6-8 weeks old female NOD scid gamma (NSG) (RRID:IMSR_JAX:010636) mice were inoculated with 4T1 cells in the Mammary fat pad. (0.5×10^6 cells). Mice were sacrificed after 14 d. A subgroup of experimental animals received Sildenafil (Molekula group, 50 mg/kg/day in drinking water. Tumor volumes were measured at the end of each experiment using a caliper and weighed. Additionally, Lungs were extracted and immediately fixed in 4% paraformaldehyde for metastasis detection. Lung metastases were counted in each group.

DU-145 primary tumor experiments:

6–8-week-old male Athymic Nude-Foxn1nu (RRID:IMSR_ENV:HSD-069) mice were inoculated with DU145 cells in the Right flank. (1×10^6 cells). Mice were sacrificed after 38d. A subgroup of experimental animals received Sildenafil (Molekula group, 40 mg/kg/day via oral gavage every other day), Lovastatin (Molekula group, 25 mg/kg, via oral gavage every other day) or both, while the remaining mice received a control gavage. Tumor volumes were measured using a caliper during the experiment and weighed at the end.

Mice were monitored for detection of humane endpoints, which were determined using a scoring sheet as follows: tumor size of 1.8 cm3, loss of ability to ambulate, labored respiration, surgical infection, or weight loss over 10% of initial body weight. For all experiments, the maximum permitted tumor volume was 1.8 cm3 and this limit was not exceeded in any experiment.

Survival plot

Kaplan-Meier survival curves (time is measured in days on the x-axis) of NPC1 gene expression in TCGA breast cancer 1075 patients. p-Values were determined using the log-rank test to compare the overall survival probability between patients with high (in red) and low (in blue) NPC1 expression.

Differential Expression Analysis in Cancer Cell Lines

Publicly available RNA sequencing (RNA-seq) count data for cancer cell lines were obtained from the DepMap portal (DepMap 2024) (https://depmap.org/portal). Cancer cell lines from breast (BRCA), lung (LUAD), colon (COAD), and prostate (PRAD) cancer types were stratified into three groups: (i) non-cancerous cell lines (n=9), (ii) highly sildenafil-sensitive cancer cell lines (n = 53), and (iii) lowly sildenafil-sensitive cancer cell lines (n = 53). Sensitivity classification was based on area under the curve (AUC) values from CTD² drug-screening data available through the DepMap portal, where cancer cell lines in the bottom quartile were classified as highly sensitive and those in the top quartile as lowly sensitive. Differential expression analysis was performed using the DESeq2 R package, comparing (a) non-cancerous vs. highly sensitive cancer cell lines and (b) non-cancerous vs. lowly sensitive cancer cell lines. Genes were considered differentially expressed (DEGs) if they met the statistical threshold of FDR ≤ 0.05. To refine the final gene set, only DEGs unique to comparison (a) were retained, ensuring specificity to the highly sensitive phenotype. Gene Ontology (GO) Biological Process enrichment analysis was performed separately for upregulated and downregulated genes using the ClusterProfiler R package (RRID:SCR_016884).

Differential Expression Analysis in TCGA Cohorts

For patient-derived tumor samples, RNA-seq data from The Cancer Genome Atlas (TCGA) were analyzed, focusing on 129 genes associated with lysosomal transport (GO:0007041). Differential expression analysis was conducted separately for each tumor type (BRCA, LUAD, COAD, PRAD) by comparing tumor and matching normal samples using a paired Wilcoxon test on TPM-normalized expression data. Log2 fold-change values (log2FC) were computed for each gene. To identify consistently dysregulated genes across tumor types, the Robust Rank Aggregation (RRA) algorithm was applied, ranking lysosomal transport genes by their fold-change within each tumor type. Genes with an RRA probability < 0.1 were identified as consistently downregulated or upregulated, depending on the direction of the analysis. Among the selected downregulated genes, two were excluded because their consistency across tumor types was borderline.

Classification of TCGA Samples by Predicted Sildenafil Sensitivity

To infer sildenafil sensitivity in TCGA patient samples, a K-Nearest Neighbors (KNN)-based approach was employed using transcriptomic similarity to cancer cell

lines. For each TCGA cohort (BRCA, COAD, LUAD), patient and cancer cell line TPM expression data (matched by tumor type) were batch-corrected using ComBat (RRID:SCR_010974) to remove technical variation. Each patient sample was clustered individually alongside highly and lowly sildenafil-sensitive cancer cell lines, and classification was performed using the n-1 nearest neighbors (where n represents the total number of cancer cell lines). To prevent circularity in downstream analyses, all lysosomal transport genes were excluded from this classification step.

Analysis of MCF7/MCF10A lysosomal gene expression in publicly available databases

The values of lysosomal gene expression are based on Barutcu et al(15).

In-silico metabolic modeling of DepMap cell lines

Using the modern, comprehensive metabolic reconstruction of human metabolism, HumanGEM(16), we simulated metabolic states and tested the effects of gene KOs in the Dependency Map (DepMap)(17) cell lines. Cell lines were chosen to include the four main cancerous ones tested in the manuscript as well as all non-cancerous ones with gene expressions from the DepMap database. Cancerous cell lines were then chosen at random from the database to achieve equal pairs of non-cancerous and cancerous breast, lung, and prostate cell lines. These cell lines and their features are summarized in **Supplementary Table 2**.

To simulate the metabolic state, the gene expression of each cell line was integrated into the HumanGEM metabolic model using the Integrative Metabolic Analysis Tool (iMAT)(18) along with media constraints. all uptake reactions for media set to -1000 simply to simulate the presence of media metabolites) to create context-specific metabolic models. Two objectives were of interest for measuring *in-silico*: growth and migration. Growth was simulated using the standard biomass reaction MAR13082. Migration is not inherently included in the HumanGEM, thus a custom reaction accounting for ATP hydrolysis, GTP hydrolysis, and NADPH usage was used to approximate cellular migration (**Supplementary Table 3**). To ensure that growth and migration could be measured from the context-specific models, both objectives were forced into the model along with the ATP maintenance reaction (MAR03964) via a small lower bound representing a small fraction of the unconstrained, optimal flux (0.01 for biomass, 0.1 for ATPM, and 0.01 for migration). From these “wild-type” (WT)

models, Sildenafil ("Sild") models were created by KO-ing the aforementioned reactions. Both the WT and Sild models were then sampled via ACHR sampling to generate 2500 representative flux states, 200 of which (every 10^{th} after 500 to reduce bias) were kept for downstream analysis.

To simulate the effects of KOs, the growth and migration objectives' fluxes were calculated before and after blocking the relevant reactions (**Supplementary Table 3**). Calculation of such objectives were done by optimizing the flux of each reaction using standard Flux Balance Analysis (FBA)(19). To directly compare the growth/migration of two models (e.g. one "WT" model and one "KO" model), linear Minimization of Metabolic Adjustment[6] (lMOMA) was utilized to first derive a flux state closest to the "KO" model starting from the "WT" state. This was particularly useful when comparing the growth/migration of sampled flux states because any perturbation/KOs would render the model infeasible. For any given flux sample state, the fluxes were mapped to the sampled model (becoming the "WT" state), and the metabolic dysregulation knock-downs were applied to the WT model (becoming the "KO" state).

Molecular Docking

The Schrödinger suite 2024 prepared the protein, generated grids, prepared the ligand, performed molecular docking against the NPC1 protein, and conducted Molecular Dynamics (MD) simulations (Schrödinger, Inc., New York, USA, RRID:SCR_014879).

Protein preparation

The crystal structure of NPC1 in a complex with cholesterol was used for molecular docking investigations and MD simulations. The Protein Data Bank (www.rcsb.org) was used to retrieve the three-dimensional crystal structure at a resolution of 1.8 Å (PDB: 3GKI) *(20)*.

To check the validity of the downloaded crystal structures, the Ramachandran plot module was utilized to construct a Ramachandran plot. The validated PDB structure was prepared using Maestro's Protein Preparation Wizard module, which included removing water molecules and adding missing residues and hydrogen atoms. The prepared protein structure was protonated at physiological pH.

Ligand preparation

The ligands (cholesterol, cGMP, and 8-pCPT-cGMP) were then subjected to energy minimization utilizing Maestro's Ligprep module and the OPLS4 force field (OPLS4, Schrödinger, Inc., New York, NY, 2021*(21)*.

Induced-Fit Docking.

Molecular docking of NPC1 to the different molecules was carried out in Schrödinger Maestro Suite 2024 using Induced Fit Docking (IFD) docking*(22)*. IFD accounts for receptor flexibility in ligand-receptor docking by iteratively combining rigid receptor docking using Glide*(23),(24)* with protein structure prediction and refinement using Prime[yellow] to predict the conformation of protein-ligand binding complexes accurately.

Molecular Dynamic (MD) simulations

MD simulation was performed using a DESMOND module by Schrödinger LLC software [desmond-yellow]. (Schrödinger, LLC, New York, NY, 2024). IFD docking solutions provided the starting state for the protein-ligand pairs, and for the cholesterol, its crystal structure 3KGI was used for the MD simulation. Each protein-ligand complex was immersed in an orthorhombic box of the SPC solvent model through the system builder panel. The solvated system was neutralized using counter ions, and a physiological NaCl salt concentration of 0.15 M. OPLS4 force field was utilized*(21)*. The simulation was 500 ns using NPT assemble class at a temperature of 300 K and atmospheric pressure of 1.01325 bar. Finally, to do a comprehensive examination, trajectories of simulated systems were generated. Using the Desmond module of the Schrödinger program, the following metrics were measured at various points along the trajectory: the root-mean-square deviation (RMSD), the root-mean-square fluctuation (RMSF), and the protein secondary structure elements (SSE). RMSD displays the variation in a protein atom's structure during molecular simulation. A low RMSD indicates a more stable system in a simulation result. The Root Mean Square Fluctuation (RMSF) is useful for characterizing local changes along the protein chain. SSE, such as alpha-helices and beta-strands, is monitored throughout the simulation.

For mutation analysis, simulations and analyses were conducted using Schrödinger software. The mutations were based on the structure 3GKI (PDB code).

Surface plasmon resonance experiments:

SPR experiments were performed using a Biacore® S200 system at 25 °C with a flow rate of 50 µl/min in buffer A (50 mM MES, pH 5.0, 150 mM NaCl, 0.02% Tween-20).

The purified protein (Cusabio, SB-YP015974HU, Recombinant Human NPC intracellular cholesterol transporter 1) was covalently coupled to a CM5 sensor chip with about 1500 response units using an amine coupling kit (Cytive) with PBST as the running buffer. A series of concentrations of Guanosine 3',5'-cyclic monophosphate (cGMP) flowed over the chip surface. The binding kinetics were analyzed with Biacore Insight Evaluation Software (v 4.0.8.19879).

Essentiality plot:

To identify potential synthetic lethality pairs between PDE5a and NPC1, we used the data from the Broad Institute DepMap project. In this study, a potential synthetic lethality gene pair A-B is defined as a gene A whose essentiality is correlated with the expression level of gene B. To establish the correlation between essentiality and expression, CCLE expression data and CRISPR gene effect data of cell lines are downloaded from the DepMap Public 22Q2 release. To validate the role of PDE5a as a synthetic lethality partner of NPC1, we tested the essentiality of PDE5a for NPC1 using the SELECT pipeline.

Analysis of the Clalit patients' data

Explorative analysis of Clalit data

Cohorts' definitions:

Lung cancer – male patients with a diagnosis of lung cancer (all stages, all histological subtypes) between the years 2002-2019 were included in the lung cancer cohorts. Cohort 1: Lung cancer patients also treated with Viagra (Sildenafil citrate) at least 6 months pre-diagnosis (N= 2388). Cohort 2: Lung cancer patients without any treatment with Viagra from 6 months pre-diagnosis to 5 years post-diagnosis (N= 11,690). Cohort 3: Lung cancer patients also treated with Vardenafil at least 6 months pre-diagnosis (N= 637). Cohort 4: Lung cancer patients also treated with Tadalafil at least 6 months prior to diagnosis (N= 1353). Cohort 5: Lung cancer patients without any treatment with a PDE5 inhibitor from 6 months pre-diagnosis to 5 years post-diagnosis (N= 10,985). Cohort 6: Lung cancer patients also treated with SSRIs at least 6 months pre-diagnosis (including citalopram, escitalopram, paroxetine, fluoxetine, sertraline, fluvoxamine, vortioxetine) (N= 3298). Cohort 7: Lung cancer patients without any treatment with Viagra or SSRIs from 6 months pre-diagnosis to 5 years post-diagnosis (N= 8392).

Cohort definitions for prostate cancer - Male patients with a diagnosis of prostate cancer (all stages, all histological subtypes) between the years 2002 and 2019 were included in prostate cancer cohorts. Cohort 1: Prostate cancer patients also treated with Viagra (Sildenafil citrate) at least 6 months pre-diagnosis (N= 7752). Cohort 2: Prostate cancer patients without any treatment with Viagra from 6 months pre-diagnosis to 10 years post-diagnosis (N= 20026). Cohort 3: Prostate cancer patients also treated with Vardenafil at least 6 months pre-diagnosis (N= 2713). Cohort 4: Prostate cancer patients also treated with Tadalafil at least 6 months pre-diagnosis (N= 5490). Cohort 5: Prostate cancer patients without any treatment with a PDE5 inhibitor from 6 months pre-diagnosis to 10 years post-diagnosis (N= 17869). Cohort 6: Prostate cancer patients also treated with SSRIs at least 6 months pre-diagnosis (including citalopram, escitalopram, paroxetine, fluoxetine, sertraline, fluvoxamine, vortioxetine) (N= 6208). Cohort 7: Prostate cancer patients without any treatment with Viagra or SSRIs from 6 months pre-diagnosis to 10 years post-diagnosis (N= 13818). Cohort 8: Prostate cancer patients also treated with Papaverine at least 6 months pre-diagnosis (N= 4782). Cohort 9: Prostate cancer patients without any treatment with Papaverine from 6 months pre diagnosis to 10 years post diagnosis (N= 22996).

Colon cancer – male patients with diagnosis of colon cancer (all stages, all histological subtypes) between the years 2002-2019 were included in the colon cancer cohorts. Cohort 1: Colon cancer patients also treated with Viagra (Sildenafil citrate) at least 6 months pre-diagnosis (N= 7938). Cohort 2: colon cancer patients without any treatment with Viagra from 6 months pre-diagnosis to 10 years post-diagnosis (N= 26,783).

Survival analysis for each cancer type: percentage of patients alive at the end of every year (0= time of diagnosis) was calculated, and a survival curve was created as an X-Y plot of %live patients at each year.

Statistical analysis for individual data using Clalit Health Servives (CHS) EMR

Descriptive statistics using chi-square for categorical variables and Ttest for continuous variables were presented.

Cox proportional hazards models were fit for each outcome, adjusting for the abovementioned potential confounders. Hazard ratio (HR) with 95% confidence intervals were reported as a measure of association.

The Cox model included some variables that were already used for the matching process for two reasons.

Missing data are rare in the CHS database; in general, they are less than 5%. However, for BMI, we have 7% missing. Thus, we decided to impute a normal value to all the missing BMI data. To verify that we didn't introduce any bias, we analyzed the missing BMI values as a separate group and found they didn't differ from the normal group.

Furthermore, to confirm the study results, we used Papaverine as a negative control to assess the association between Sildenafil and statin use and survival rate among cancer patients, given that it might be an unobserved confounder. Papaverine was chosen to be a variable because it has no effect on the outcome of interest but is subject to the same unobserved confounding as the exposure of interest.

Study design and population.

We conducted a retrospective cohort study using CHS-EMR data to estimate the association between statin and Sildenafil use within 6 months prior to cancer diagnosis and 5-year survival. CHS is the largest integrated payer-provider healthcare organization in Israel. CHS has a comprehensive healthcare data warehouse that combines hospital and community medical records, laboratory and imaging information, and vital status (alive, dead), which can be accessed for use in observational and epidemiologic studies(25),(26). Membership turnover within CHS is less than 2% annually(27), facilitating the study of population health trends over time. Data on cancer diagnoses were obtained from the Israeli National Cancer Registry and merged with CHS's electronic medical record using ID number, full name (personal name and family name), and date of birth.

This study included CHS members who had a cancer diagnosis, aged 35-65 years old, between 2008 and 2017, with at least 12 months of continuous membership.

All study participants were followed until the first occurrence of any of the following within five years of cancer diagnosis: (1) death, (2) loss of follow-up (due to change in membership), (3) end of follow-up (i.e. defined as being alive at the fifth year of cancer diagnosis).

Study variables

Exposure variable was categorized into 5 groups of statin use or Sildenafil use within 6 months prior to index date: (i.e. cancer diagnosis date): (1) Having at least one dispensation of statin; (2) Having 1 or 2 dispenses of Sildenafil; (3) at least 3 dispenses of Sildenafil; (4) Having both at least one dispensing statin and 1 or 2 dispensing of Sildenafil; and (6) Having both at least one dispensing statin and at least 3 dispenses of Sildenafil

For medication usage data, information was extracted from dispensing records, which occur after a prescription is issued. Health insurance covers the cost of Statins and Viagra. While it is known that the purchase of Viagra is expensive, it is not an issue within the Israeli health care system, since it is covered by health insurance, and we are only including individuals who have had a dispensing; the cost burden is mitigated through the national healthcare coverage.

The outcome variable was defined as the 5-year survival rate.

Confounders and confounders adjustment

Adjustments were performed in two stages. First, the exposed and the non-exposed patients were matched on an initial set of potential confounders. Covariates included in the analysis were based on the input of domain experts and scientific literature related to the factors associated with the survival rates and the likelihood of using statin or Sildenafil. To adjust for the baseline differences between those who used Sildenafil or statins, we employed both nearest–k neighbor and exact matching approach. In the Sildenafil exposure groups, we set the ratio of treated to untreated patients at 1:5. Using matching techniques, we ensure balance between the exposed and non-exposed groups based on potential confounders.

Subjects were matched based on age; sex; population sector (Jewish, Arab, Ultra-Orthodox); socioeconomic status (SES, based on place of residence and categorized into 3 levels, low, medium, high); body mass index (BMI as a categorical variable); and type of malignancy. Further adjustment was performed using Cox proportional hazards regression to account for potential confounders. Confounders that were adjusted for in the Cox model included: smoking status, systolic and diastolic blood pressure, having comorbidities (diabetes, ischemic heart disease, fatty liver, kidney failure, asthma, Chronic obstructive pulmonary disease, and Peripheral artery disease), and having medication use (nitrates, ACE inhibitors, beta blockers, Aldosterone antagonists, Anti thrombotic, and Digitalis Glycosides, that were defined as dispensing of each specific treatment within 12 months prior to index date. Comorbidities were extracted using ICD-9 codes, and we included the most recent value prior to the index date. Medications were extracted using ATC-5 codes. The Cox regression included some of the variables used in matching to better control for residual confounding, since we did not use exact matching for all variables.

We acknowledge that certain factors, such as cancer stage at diagnosis year, could potentially influence both medications use and the outcome. However, due to data limitations, we were unable to include cancer stage as a confounder in our analysis. Instead, we focused on baseline chronic conditions, which are strong indicators of health status and are associated with both medications use and the outcome. These chronic conditions were carefully considered in our analysis to adjust to underlying health status. We believe that these baseline factors capture important aspects of the patient's health that could influence both treatment patterns and survival outcomes.

As a sensitivity analysis, we conducted the same study specifically on patients with Type 2 diabetes to confirm Sildenafil use, given that this group is more likely to have Sildenafil documented in their electronic medical records (EMR) and to use the medication. We excluded diabetes as a confounder in this analysis. Additionally, we performed the same analysis using Papaverine as a negative control exposure.

A further sensitivity analysis was conducted, limiting the study population to males only. We have conducted the same matching process and statistical analysis.

Ethics

All animal experiments complied with ethical regulations and were approved by the Weizmann Institute Animal Care and Use Committee. Following the US National Institute of Health, the European Commission, and the Israeli guidelines (IACUC 00520124, 208311022, 100620122-2 and 04330523-1).

These human data analyses were conducted in accordance with the Declaration of Helsinki of Clalit Health Services (CHS)- Helsinki approval no. # 0068-23-COM2 and approved by the Institutional Review Board (IRB), (COM2-0068-23), and the Weizmann IRB 2704-1. Due to the retrospective nature of the study, informed consent was waived. For human TNBC sample Experiments, written informed consent was obtained from patients (approval number: 0413-13-RMC**)**.

Statistics and reproducibility

The sample size was chosen in advance, in accordance with the described experiment's common practice, and is reported for each experiment. Statistical tests were performed using the Prism GraphPad statistics function. $P \leq 0.05$ was considered significant in all analyses ($^{*}P < 0.05$, $^{**}P < 0.01$, $^{***}P < 0.001$). Unless specified otherwise, each experiment was conducted with at least three biological replicates repeated at least three times. All error bars represent SD. NS, not significant, $^{*}P \leq 0.05$, $^{**}P < 0.01$, $^{***}P < 0.001$, $^{***}P < 0.0001$, unless noted otherwise.

Data availability statement

The RNA-seq data discussed in this publication has been deposited in NCBI's Gene Expression Omnibus and are accessible through GEO series accession number GSE334363. The TCGA data analyzed in this study were obtained from the Genomic Data Commons (GDC) data portal at https://portal.gdc.cancer.gov/.

Requests for access to all or parts of the Clalit datasets should be addressed to Clalit Healthcare Services via the Clalit Research Institute and addressed to Professor Shay Ben-Shachar at shayb@clalit.org.il. Requests will be considered by the Clalit Data Access Committee per the Clalit data-sharing policy. All other raw data generated in this study are available upon request from the corresponding author.

Results

Decreasing PDE5a activity restricts cancer migration and metastasis formation, and benefits patients' survival

To evaluate the potential role of cGMP in carcinogenesis, we chose three different types of cancer cells for which there is an orthotopic mouse model- breast (4T1), lung (LLC), and colon (MC38). Across all three types of cancer, sildenafil rapidly increased cGMP activity, as evidenced by increased levels of phospho-VASP 239(28) (**Figure 1A**). In vivo, sildenafil raised plasma cGMP levels in both Balb/c and C57BL/6 mice (**Figure 1B**). Notably, in all three cancer models, sildenafil treatment reduced cell viability, colony formation, and migration in vitro to varying degrees, while it markedly restricted lung metastases in vivo (**Figure 1C-E** and **Supplementary Figure 1A**). To further dissect the cancer-specific effects of sildenafil, we continued with the 4T1 breast cancer model, which exhibited the most pronounced response and highest sensitivity to treatment among the three systems evaluated. Using the 4T1 breast cancer model(29), we distinguished sildenafil's effects on primary tumors versus metastases and found that, while sildenafil had minimal impact on primary tumor growth, it significantly reduced the formation of lung metastases (**Figure 1F**). Next, we compared, in silico, the proliferation and migration objectives of DepMap noncancerous and cancerous cell lines using genome-scale metabolic modeling. We found that while cancer cells display both higher proliferation and migration rates than noncancerous cells, sildenafil predictably significantly impairs cancerous migration (**Figure 1G**). These findings suggest that sildenafil primarily targets metastatic progression rather than primary

tumor growth. Moreover, the robust in vivo efficacy observed across all cancer lines, in contrast to the variable effects seen in vitro, suggests that sildenafil likely affects multiple steps in metastasis rather than the individual processes assessed in vitro.

To confirm that the restricted cancerous features we found are specific for PDE5a inhibition, we validated that vardenafil, another FDA-approved PDE5a inhibitor(30), also inhibited 4T1 breast cancer viability, migration, and colony formation (**Supplementary Figure 1B-D**). To verify that these anti-cancer effects are not an off-target effect of sildenafil and vardenafil, we knocked down PDE5a levels in 4T1 cells using 2 different shRNAs (**Supplementary Figure 1E-F**). Like sildenafil, shPDE5a significantly reduced the viability and migration of cancer cells (**Supplementary Figure 1G-H**). To exclude reduced cell viability as a confounding factor, we performed a transwell migration assay, which demonstrated that sildenafil reduced cell migration independently of its effects on cell viability (**Supplementary Figure 1I**). Furthermore, mice injected with shPDE5a-expressing cancer cells developed significantly fewer lung metastases than those injected with shGFP-expressing cells (**Supplementary Figure 1J**). No further reduction of the phenotypes was observed when different clones of shPDE5a cancer cells were treated with sildenafil, suggesting that sildenafil specifically targets PDE5a (**Supplementary Figure 1G-H**). In addition, when 4T1 cancer cells were injected into Non-Obese Diabetic severe combined immunodeficient gamma (NSG) mice, sildenafil treatment again resulted in fewer lung metastases (**Supplementary Figure 1K**). The overlap between genetic PDE5a knockdown and pharmacologic inhibition, together with efficacy in NSG mice, suggests that by inhibiting PDE5a, sildenafil induces a non-immune, anti-tumorigenic intrinsic effect.

To assess the human relevance of our findings, we first tested the effect of sildenafil in human breast (MDA-231), prostate (DU-145), colon (HCT-116), and lung (A549) cancer cells. Similar to our results with mouse cancer cells, sildenafil restricted viability and migration in all the tested human cancer cells (**Supplementary Figure 1L-M**). Second, we utilized data from Clalit Health Services (CHS) Electronic Medical Records (EMR), which encompasses 20 years of health records for 5 million individuals(31). Our exploratory analysis revealed that sildenafil use is associated with improved survival in male patients with colon or lung cancers, further supporting the potential relevance of these findings to human cancer patients (**Figure 1H**). To validate that the

specificity of sildenafil's protective effect on cancer patients' survival is caused by PDE5a inhibition, we further analyzed the data of prostate cancer patients for whom we had an adequate number of patients who were taking different PDE inhibitor drugs. Our analysis revealed that, in addition to sildenafil, other available PDE5a inhibitor drugs, such as tadalafil and vardenafil, also enhanced survival in prostate cancer patients (**Supplementary Figure 1N**). Conversely, inclusion of a negative-control exposure to assess specificity, using the PDE10A inhibitor papaverine revealed no comparable survival benefit (**Supplementary Figure 1O**).

Collectively, these findings demonstrate that the specific inhibition of PDE5a by sildenafil effectively restricts cancerous features and may offer therapeutic benefits for cancer patients.

Inhibiting PDE5a activation in cancer induces cholesterol synthesis and accumulation, decreasing cholesterol availability

To gain a broad understanding of how sildenafil restricts metastasis, we performed RNA sequencing on 4T1, LLC, and MC38 cells treated with sildenafil. Strikingly, in all 3 cancer cells, the primary pathways and genes upregulated were related to cholesterol biosynthesis genes (**Figure 2A and Supplementary Figure 2A**). Cholesterol synthesis is a tightly regulated, multi-step metabolic pathway that begins with sterol regulatory element-binding protein 2 (SREBP2), the key transcription factor that regulates the expression of cholesterol biosynthesis genes(32) (**Supplementary Figure 2B**). When cellular cholesterol levels are low, the SREBP2 precursor is cleaved into its mature form, which translocates to the nucleus and promotes the transcription of enzymes involved in cholesterol synthesis. The cholesterol synthesis process initiates with the condensation of acetyl-CoA molecules to form HMG-CoA (3-hydroxy-3-methylglutaryl-CoA), catalyzed by the enzyme HMGCS1. HMG-CoA is then reduced to mevalonate by HMGCR (HMG-CoA reductase), the rate-limiting enzyme in the pathway and a major regulatory checkpoint(32). This step is the primary target of statins, which are widely used cholesterol-lowering drugs. The synthesized cholesterol can then be incorporated into membranes or esterified by Acetyl-CoA: Cholesterol Acyltransferase 2 (ACAT2)(33) for storage in lipid droplets (LD). Consistent with reports of constitutive nuclear SREBP2 expression in cancer cells(34,35), we observed nuclear localization of SREBP2 in 4T1 breast cancer cells, which was further increased following sildenafil treatment and associated with a significant upregulation of

downstream cholesterol biosynthesis genes (**Figure 2B-C)**. Given these marked effects on cholesterol synthesis pathways, we employed mass spectrometry metabolic analysis to measure total and esterified cholesterol levels in cancer cells, using lovastatin, an established HMG-CoA inhibitor(36), as a comparison. We found that while both sildenafil and lovastatin reduced free cholesterol levels, sildenafil increased cholesterol ester levels, whereas lovastatin reduced them (**Figure 2D**).

We further corroborated the increase in expression of cholesterol genes at both the RNA and protein levels in 2D and 3D cultures of multiple murine and human cancer cells (**Supplementary Figures 2C-H**). Notably, the increase in cholesterol synthesis genes' expression was significantly lower in untransformed hepatic, mammary, and epithelial cells compared to the cancerous cells, suggesting that sildenafil specifically disrupts cholesterol metabolism in cancer cells (**Supplementary Figure 2I-J**). In addition, we confirmed that the upregulation of cholesterol biosynthesis genes results directly from PDE5a inhibition, as both shPDE5a knockdown and vardenafil treatment produced a comparable increase in 4T1 breast cancer cells (**Supplementary Figure 2K-M**). Finaly, to assess clinical relevance, we treated primary human breast cancer cells derived from patient biopsies with sildenafil. Similar to our findings in cancerous cells, sildenafil treatment in three independent breast patient samples upregulated the expression levels of enzymes involved in cholesterol synthesis and induced the levels of cholesterol esters, accompanied by a decrease in free cholesterol, highlighting sildenafil's potent effect in limiting cholesterol availability while increasing its storage potential (**Figure 2E and Supplementary Figures 2N-P**).

Increasing cGMP levels decreases cellular cholesterol availability and perturbs cellular membranes

To determine whether the increase in cholesterol synthesis is a direct consequence of cGMP activation, we used the cGMP activator Lificiguat (YC-1)(37). First, we demonstrated that 50μM YC-1 induces pVASP/VASP activation comparable to that observed with 50μM sildenafil (**Figure 2F**). Next, using a cGMP fluorescence probe, we showed that the increase in pVASP/VASP following YC-1 treatment correlates with the corresponding elevation in cGMP levels (**Supplementary Figure 3A**). Notably, similar to sildenafil, YC-1 treatment resulted in upregulation of the cholesterol-synthesis rate-limiting enzyme gene, 3-hydroxy-3-methyl-glutaryl-coenzyme A reductase (HMGCR) (**Supplementary Figure 3B**). To explore the morphological

effects of high cholesterol synthesis, we co-stained 4T1 breast cancer cells with the cholesterol marker, Filipin, and the lipid droplet (LD) marker, BODIPY. We found an accumulation of cholesterol and LD in cancer cells treated with sildenafil, suggesting a potential trafficking defect following cGMP induction (**Figure 2G**). Staining sildenafil-treated cells with the cholesterol probe, D4-EGFP(14,38), further confirmed the accumulation of cholesterol (**Supplementary Figure 3C**). Likewise, knockdown of PDE5a and YC-1 treatment demonstrated cholesterol accumulation and LD elevation (**Figure 2H and Supplementary Figure 3D-E**).

Since cholesterol ester lipase (CEL) and ACAT2 (SOAT2)(33,39) mediate the breakdown of lipid esters and the conversion of cholesterol into cholesterol esters, respectively, we measured the expression levels of these enzymes. While we found no change in CEL expression, ACAT2 levels increased significantly (**Supplementary Figure 3F**). Thus, the increase in cholesterol ester accumulation following sildenafil treatment was due to upregulation in cholesterol-synthesizing enzymes rather than a perturbed degradation. Notably, as with differences in cholesterol synthesis gene expression between cancerous and non-transformed cell lines, sildenafil induced cholesterol accumulation exclusively in cancerous cell lines. (**Supplementary Figure 3G**).

We next conducted an unbiased lipidomic to specify the effect of PDE5a inhibition on cholesterol metabolism in cancer. A detailed analysis of the lipidomic data following sildenafil treatment revealed a specific elevation in triglycerides (TGs), a reduction in phosphatidylcholines (PCs), and an increase in Bis(monoacylglycerol)phosphate (BMP) levels (**Figure 2I and Supplementary Figure 3H-I**).

Cholesterol is primarily utilized by the plasma membranes(40). Specifically, in cancer, membrane lipid rafts play a crucial role in cytoskeletal cell signaling and migration(41,42). Disrupting lipid-raft–dependent signaling and membrane organization is expected to reduce metastatic potential, as both are essential for invasion, intravasation, endothelial adhesion, colonization, and outgrowth at distant sites. Indeed, we found that sildenafil decreases the number of lipid rafts, as exemplified by staining with lipid raft marker Cholera Toxin Subunit B (CTSB) (**Figure 2J**). Furthermore, using methyl-β-cyclodextrin (MβCD), an amphipathic polysaccharide known to deplete membrane cholesterol(43), we show that sildenafil and MβCD induce comparable depletion of plasma membrane cholesterol and, consequently, similar

inhibition of cancer cell migration, supporting the notion that sildenafil restricts metastasis by altering plasma membrane properties (**Supplementary Figure 3J-K**). Notably, combining sildenafil and cholesterol restored lipid raft formation (**Supplementary Figure 3J**).

Moreover, since cholesterol is also essential for the membranes of intracellular organelles, such as the mitochondria(44), we assessed the mitochondrial functional profile. Similar to other agents that disrupt mitochondrial membrane potential, where basal OCR is already near the uncoupled state due to membrane depolarization(45), we found that sildenafil-treated cancer cells exhibited reduced basal respiration and ATP production, accompanied by increased mitochondrial reactive oxygen species (MitoROS), indicating mitochondrial dysfunction (**Figure 2K and Supplementary Figure 3L**).

To confirm that cancer cells experience a significant reduction in endogenous cholesterol availability following sildenafil treatment, we supplemented 4T1 cells treated with sildenafil with exogenous cholesterol. We found that cholesterol supplementation in sildenafil-treated cancer cells significantly reduced cholesterol synthesis gene expression and restored cancer cell viability and migration (**Figure 2L and Supplementary Figure 3M-N**). Consequently, decreased endogenous cholesterol synthesis following exogenous cholesterol addition reduced lipid droplet accumulation (**Figure 2M**).

Thus, in cancer cells, sildenafil treatment decreases cholesterol availability for both plasma and organelle membranes, thereby impairing lipid raft formation and mitochondrial ATP production. Concurrently, cholesterol synthesis and ester formation increase, leading to an accumulation of cholesterol in LD.

Downregulation of PDE5a leads to cholesterol accumulation in lysosomes and a compensatory increase in endogenous cholesterol production

The morphological and lipidomic profiles observed following sildenafil treatment of cancer cells suggest that PDE5a inhibition and the consequent elevation in cGMP lead to increased cholesterol accumulation and decreased cholesterol availability, recapitulating features of a lysosomal storage disease(46,47). Strengthening this notion, lysosomes are well known to play a central role in cholesterol trafficking and homeostasis(48). Therefore, we next evaluated whether lysosomes contribute to

decreased cholesterol availability following PDE5a inhibitor treatment. First, we imaged cells treated with sildenafil with an electron microscope and found increased cholesterol vacuoles and crystal-like structures(39) within organelles (**Figure 3A**). Additionally, treatment with sildenafil or vardenafil was associated with increased lysosomal abundance and cholesterol accumulation in lipid droplets (**Figure 3B and Supplementary Figure 4A)**. Furthermore, in sildenafil-treated cells, Filipin staining demonstrated the co-localization of cholesterol with the Lysosomal-associated membrane protein 1 (LAMP1) and the Lysosomal transmembrane protein 192 (TMEM192) (**Figure 3C and Supplementary Figure 4B**). These data suggest that PDE5A inhibitors disrupt cholesterol export from lysosomes, thereby reducing free cholesterol availability. If so, the observed upregulation of cholesterol synthesis likely represents a compensatory response to this decrease in cholesterol availability.

Interestingly, calcium levels regulated by cGMP have been shown to be essential for the sterol-sensing mechanism of SREBP2 in regulating cholesterol synthesis(49,50). Indeed, we found that sildenafil increased SREBP2 activity and the expression of genes involved in cholesterol synthesis (**Figure 2B-C**). Using BAPTA-AM, a calcium chelator, we evaluated whether decreasing calcium levels could interfere with the consequential effects of sildenafil on cholesterol metabolism. We found that co-administration of sildenafil and BAPTA-AM significantly blocked the sildenafil-induced expression of cholesterol-synthesizing genes at both the RNA and protein levels (**Supplementary Figure 4C-D**). Notably, although BAPTA treatment did not significantly reduce lysosomal cholesterol accumulation (**Supplementary Figure 4E**), combined treatment with BAPTA-AM and sildenafil increased cancer cell death, likely by blocking a compensatory increase in cholesterol synthesis aimed at restoring cholesterol availability (**Supplementary Figure 4F**).

In addition, given the strong link between LSDs, decreased cholesterol availability, and autophagy, we evaluated for autophagy by measuring p62, LC3-I to LC3-II conversion, and quantifying LC3 vesicles using Western blot analysis and immunofluorescence(51). We found that sildenafil treatment significantly increased p62 and LC3-II levels in a time-dependent manner (**Figure 3D-F**). These data indicate that by promoting cholesterol accumulation, sildenafil impairs lysosomal degradative capacity, leading to p62 accumulation. To determine whether the observed autophagy defects represented enhanced autophagosome formation or impaired degradation, we

employed the lysosomal V-ATPase inhibitor, Bafilomycin A1 (BafA1), a compound that blocks autophagic flux by preventing lysosomal degradation. Notably, combining BAFA1 with sildenafil did not significantly alter LC3B or p62 accumulation (**Figure 3G**), suggesting that sildenafil treatment acts at the same late stage as BAFA1, blocking lysosomal degradation and restricting autophagic flux.

These findings led us to conclude that, following PDE5A inhibition, cholesterol accumulation within lysosomes impairs lysosomal function, including pH regulation and autophagic flux, thereby further reducing overall cholesterol availability. Next, to compensate for this deficiency, cancer cells activate calcium-dependent cholesterol synthesis by activating the transcription factor SREBP2.

Downregulation of NPC1 in cancer recapitulates PDE5a inhibition phenotype

Interestingly, the cellular phenotypes of cancer cells treated with sildenafil resemble those previously observed in Niemann Pick C (NPC1) disease, a rare monogenic metabolic lysosomal disorder wherein the cells cannot mobilize cholesterol from the lysosome for cellular utilization(52,53) . To evaluate the essentiality of NPC1 in cancer cells, we downregulated NPC1 activity in 4T1 breast cancer cells using either genetic knockdown or chemical inhibition with shNPC1, siNPC1, or U1866A(54), respectively (**Figure 4A-B**). U1866A is a small molecule that binds to NPC1 in the region responsible for recognizing and transporting cholesterol. This binding blocks NPC1's ability to transfer cholesterol to the cytosol or other organelles, resulting in cholesterol accumulation within lysosomes and secondary defects in membrane trafficking and autophagy(55). We confirmed that in cancer cells, the treatment with sildenafil, the knockdown of NPC1, and the usage of NPC1-inhibitor U1866A(54) resulted in lysosomal accumulation of cholesterol (**Figure 4C**). Furthermore, measuring the lysosomal pH using the ratio-metric probe, LysoSensor(56,57), we found that both U18666A treatment and sildenafil increased lysosomal pH (**Figure 4D**). Indeed, the NPC1 inhibitor, U1866A(54), synergized with sildenafil to further reduce cancer proliferation, colony formation, and migration (**Supplementary Figure 5A-C**). Similarly to PDE5a inhibition, and as previously described in a different model, shNPC1 elevated the expression of NPC2 and cholesterol biosynthesis genes(53,58) (**Figure 4E-F**). Interestingly, PDE5a RNA was also increased following NPC1 downregulation, further supporting the notion that NPC1 and PDE5a cooperate metabolically (**Figure 4E**). Additionally, shNPC1 decreased colony growth and metastasis formation (**Figure 4G-H**). Notably, 4T1 breast cancer cells with NPC1

downregulation, treated with sildenafil, demonstrated significantly reduced proliferation and migration compared to breast cancer cells expressing NPC1 (**Figure 4I-J**). To evaluate the translational relevance of our findings, we performed a computational analysis of the TCGA database. We found that patients with cancer expressing low NPC1 levels have a longer survival than those with higher NPC1 expression (**Supplementary Figure 5D**). Furthermore, computational analysis aimed at identifying synthetic lethal interactions(59) predicted that NPC1 and PDE5a are synthetically lethal (**Supplementary Figure 5E**).

Thus, PDE5a inhibition and NPC1 deficiency produce similar cellular phenotypes in cancers, thereby restricting cancer progression and demonstrating synthetic lethality in patients, which correlates with improved survival.

The non-canonical function of cGMP in cancer disrupts cholesterol binding to NPC1

cGMP has been shown to exert biological effects via activating protein kinase G (PKG)(60). Therefore, we investigated whether sildenafil stimulates cholesterol biosynthesis through PKG signaling. We found that PKG inhibition by KT5823 did not reduce the sildenafil-induced expression of cholesterol synthesis genes and did not rescue the sildenafil impairment of cancer cells' migration (**Supplementary Figure 6A-B**). Thus, we hypothesized that cGMP impairs cholesterol trafficking by a non-canonical cGMP-dependent pathway. To delineate this pathway, we performed molecular dynamics (MD) simulations following docking studies. The MD simulation revealed that cGMP could bind to the lysosomal cholesterol transporter NPC1 at the same site as cholesterol (**Supplementary Figure 6C**). While cholesterol is hydrophobic, cGMP is hydrophilic and binds NPC1 via water molecules. Once cGMP leaves NPC1, the binding site is more hydrophilic, and cholesterol binding is less efficient (**Supplementary Figure 6D**). Based on this modeling, mutations E30A, K38A, and the aromatic residues F108A and F203A are expected to affect the binding of both cGMP and cholesterol to NPC1. Indeed, in the NPC1 (PDB: 3GKI) K38A mutant, the ligand is displaced from the binding site during an MD simulation (**Supplementary Figure 6E-G**). Likewise, F203A mutation (specifically as part of the double P202A/F203A mutation) in NPC1 was shown to abolish cholesterol binding and cause a Niemann-Pick disease phenotype in mice, including neurodegeneration, hepatic cholesterol accumulation, and early mortality(61).

Further confirming the specificity of the cGMP-NPC1 binding, Root Mean Square Deviation Values for the displacement of a selection of atoms for NPC1 protein during molecular dynamics simulation over time demonstrated that cGMP and cholesterol bound to NPC1, while the modified cGMP molecule, 8-pCPT-cGMP(62), did not (**Figure 4K**). Additionally, supplementing 4T1 breast cancer cells with 8-pCPT-cGMP in vitro did not induce cholesterol gene expression or lysosomal cholesterol accumulation (**Figure 4L-M**). Using a Surface Plasmon Resonance (SPR) assay, we confirmed the predicted cGMP-NPC1 binding in a dose-dependent manner (**Figure 4N**). Together, these results imply that cGMP directly binds to NPC1, reducing its interaction with cholesterol and thereby limiting cholesterol availability.

Cancer cells express low levels of lysosomal genes and a higher sensitivity to sildenafil

To understand the higher sensitivity of cancer cells to sildenafil compared to normal cells, we analyzed publicly available datasets. First, we analyzed a collection of RNA expression profiles of cancer cell lines treated with sildenafil as part of the Cancer Target Discovery and Development (CTD^2) Network for drug screening within the DepMap database. We divided the data into two groups based on high and low sensitivity to sildenafil. We performed a differential expression analysis between these two groups and non-cancerous cell lines, focusing on genes that are significantly differentially expressed (DeSeq2 analysis, FDR < 0.05) only within highly sensitive cancer cells compared to non-cancerous ones (private-highly-sensitive DEGs) (**Figure 5A**). We found significant downregulation of lysosome/vacuole transport genes in cancer cells with high sensitivity to sildenafil (**Figure 5B**). Furthermore, analysis of TCGA cohorts encompassing breast, colon, lung, and prostate cancers demonstrated that tumors predicted to be highly sensitive to sildenafil exhibited a significant and consistent downregulation of lysosomal genes, both collectively and individually, when compared with their matched adjacent normal tissues (**Figure C-D**). Furthermore, DepMap cell line modeling using genome-scale metabolic simulations of combining sildenafil treatment with lysosomal transporter knockout consistently produced larger reductions in flux migration in cancer cells than in non-cancerous cells (**Figure 5E**).

To validate these findings in our models, we performed a focused analysis of publicly available datasets(15) and confirmed our results using quantitative PCR, which showed that MCF7 cancer cells express lower levels of lysosomal genes compared to

untransformed MCF10 cells, suggesting that reduced lysosomal gene expression may be associated with malignant phenotypes (**Figure 5F-G**). To confirm the implications of this analysis, we overexpressed LAMP1, a lysosomal gene identified as downregulated in the analysis above, in MCF7 cells and treated the cells with sildenafil (**Figure 5H**). We found that overexpression of LAMP1 alone reduced the malignancy of the cancer cells, as evidenced by decreased migration (**Figure 5I**). Notably, combining LAMP1 overexpression with sildenafil treatment significantly reduced the cells' sensitivity to sildenafil (**Figure 5I**).

Thus, the intrinsic downregulation of lysosomal genes in cancer cells and tumors, compared with untransformed cells and adjacent normal tissues, contributes to sildenafil sensitivity, likely by amplifying the reduction in cellular cholesterol availability induced by increased cGMP binding to NPC1.

Combined sildenafil and statin treatment is associated with longer survival in cancer patients

Since sildenafil-induced lysosomal cholesterol accumulation limits cholesterol availability in cancer cells, we investigated the potential therapeutic synergy between sildenafil and lipid depletion to further restrict cancer survival. In silico analysis, using genome-scale metabolic modeling of select DepMap cancer cell lines, supported this notion by demonstrating the lowest migration flux in cancer cells receiving the combined treatment compared to single treatments or untreated controls (**Supplementary Figure 7A**). Next, we inhibited PDE5a in breast cancer cells supplemented with lipid-depleted medium (LDPS) or lovastatin(63,64). We found that treating 4T1 breast cancer cells with sildenafil synergized with lipid-depleted medium and lovastatin, resulting in significant inhibition of proliferation, migration, and induction of apoptosis (**Figure 6A-C and Supplementary Figure 7B-C**). Consistent with these findings, PDE5a knockdown in breast cancer cells further demonstrated reduced migration upon lovastatin treatment (**Supplementary Figure 7D**). Conversely, treating untransformed cells with sildenafil and a lipid-depleted medium did not result in significant cell death or apoptosis (**Supplementary Figure 7E**). Interestingly, immunofluorescence staining of 4T1 cells showed that treatment with sildenafil and statins, either alone or in combination, preserves the sildenafil-induced accumulation of cholesterol in lysosomes, despite the lovastatin-mediated reduction in membrane-associated free cholesterol (**Figure 6D**). Thus, sildenafil and lovastatin target distinct

steps in cholesterol metabolism, lysosomal transport, and biosynthesis, respectively, making their combined treatment synergistic in reducing cholesterol availability for cellular needs.

To further evaluate the therapeutic relevance of our findings, we treated both 4T1 and prostate cancer-bearing mice with sildenafil and statins. In both breast and prostate primary tumor models, the combined therapy significantly affected the primary tumor growth (**Figure 6E and Supplementary Figure 7F-G**). We then assessed the combined therapeutic effect on lung metastasis in breast and colon cancer models. While both sildenafil alone and the combined treatment significantly reduced lung metastases in the 4T1 breast and MC-38 colon cancer models, the additive benefit of the combination therapy varied, being more pronounced in the breast cancer model (**Figure 6F and Supplementary Figure 7H**). This may be because sildenafil exerts the primary anti-metastatic effect, whereas lovastatin targets compensatory mechanisms that are potentially less prominent in colon cancer. To specify the translational therapeutic relevance of sildenafil for cancer patients, we established a matched retrospective cohort study using Clalit Health Services (CHS) dataset to evaluate 5-year survival rates, including 40,567 male cancer patients aged 35-65 who were diagnosed between 2008 and 2017, on which we performed a two-stage adjustment; first, subjects were matched based on age, sex, population group (Jewish, Arab, Ultra-Orthodox), socioeconomic status, (categorized into three levels: low, medium, high), body mass index (BMI as a categorical variable), and type of malignancy. Based on the patients' dispensing history of sildenafil and statins within six months before the index date (i.e., before cancer diagnosis), we categorized them into six groups: no treatment, sildenafil or statins only, 1-2 sildenafil dispensations, 3+ sildenafil dispensations, 1-2 sildenafil dispensing with statins, and 3+ sildenafil dispensing with statins. **Supplementary Table 4** describes the study population by exposure status. Furthermore, we adjusted for potential confounding variables and performed survival analysis using Cox proportional hazards models (**Supplementary Table 5**).

Our results indicate that cancer patients taking sildenafil have improved survival rates compared to non-users, with a positive association between increased dosing and survival. Consistent with the existing literature(65), we also found that cancer patients treated with statins had improved survival outcomes (**Figure 6G**). Notably, we found that statin and sildenafil users have better survival rates compared to non-users,

particularly among those who reported at least three dispenses of sildenafil within six months before cancer diagnosis. Statin use was significantly associated with reduced risk compared with nonuse (HR 0.76, 95% CI 0.73–0.80). Viagra use of at least once versus nonuse was not significantly associated with risk (HR 0.92, 95% CI 0.77–1.09), whereas Viagra use 3 or more times was significantly associated with reduced risk (HR 0.74, 95% CI 0.55–0.99). In addition, combined statin use and Viagra use at least once was significantly associated with reduced risk (HR 0.81, 95% CI 0.67–0.91), and the combination of statin use with Viagra use 3 or more times showed a stronger association (HR 0.68, 95% CI 0.50–0.91) (**Supplementary Table 5**). When we limited our results to males only, the results were consistent with our main analysis. While users of both statins and one or two dispensing of sildenafil experienced a 17% decreased risk of death within five years of diagnosis [Hazard Ratio (HR): 0.83; 95% Confidence Interval (CI): 0.69-0.99] compared to non-users, those using statins with at least three dispensing of sildenafil showed a 31% decreased risk of death within five years of diagnosis [HR: 0.69; 95% CI: 0.51-0.93] compared to non-users. These results reinforce our primary findings for the entire study population and underscore the quality of our matching process and analysis (**Supplementary Tables 6-7** and **Figure 6G**).

Furthermore, we examined this relationship among Type 2 diabetic patients with cancer who are taking sildenafil, as these patients are likely prescribed sildenafil for vascular issues, underscoring their physical health challenges. Consistent with our results, diabetic patients who were taking statins and reported at least 3 dispensings of sildenafil within six months before cancer diagnosis had a 41% decreased risk of death within five years of cancer diagnosis [HR:0.59, 95%CI: 0.41-0.86] (**Supplementary Figure 8A and Supplementary Tables 8-9**). In contrast, patients receiving papaverine and statins did not have similar survival benefits, and no dose-response relation was found (**Supplementary Tables 10-11 and Supplementary Figure 8B).**

Thus, combining PDE5a inhibitors with statins mechanistically synergizes to reduce cholesterol availability, decrease metastases, and prolong survival.

Discussion and study limitations

Dynamic metabolic rewiring drives cancer progression. We show that PDE5A inhibition elevates cGMP and suppresses cancer survival, migration, colony formation, and metastasis across multiple models, primarily restricting metastatic progression. Mechanistically, cGMP binds NPC1, impairing lysosomal cholesterol export and

causing cholesterol accumulation, autophagy disruption, reduced lipid rafts, and mitochondrial dysfunction. Cancer cells were selectively vulnerable due to reduced lysosomal gene expression. Compensatory SREBP2 activation increased cholesterol biosynthesis, and combining PDE5A inhibitors with statins further reduced cholesterol availability, improving antimetastatic effects and survival outcomes (**Figure 6G-H**).

Sildenafil, widely used to treat erectile dysfunction and hypertension, has also been associated with improved outcomes in gastrointestinal cancers(66). Mechanistically, PDE5 inhibitors exert anticancer effects through multiple pathways, including elevating intracellular cGMP, activating PKG, and leading to phosphorylation and ubiquitin-mediated destabilization of oncogenic proteins such as c-MYC(67). Additionally, PDE5 inhibitors have been shown to enhance antitumor immunity (68), and improve chemotherapy delivery via enhanced tumor perfusion(67). In breast cancer, PDE5 inhibition suppresses cancer-associated fibroblast activation and cancer stem cell survival(69,70). Furthermore, PDE5 inhibitors show synergistic potential with immunotherapy and chemotherapy by overcoming tumor immunosuppression and stromal-mediated therapy resistance(67).

We find that the primary anticancer effect of sildenafil is the restriction of metastasis by reducing cholesterol availability. PDE5A inhibition disrupts cellular membranes and lipid rafts, the dynamic platforms mediating the signaling involved in migration, invasion, and survival (42,71), while also affecting lysosomal and mitochondrial function. Since metastatic cells have particularly high demands for cholesterol and ATP to support membrane remodeling and motility(72), reducing these resources preferentially limits metastatic progression over primary tumor growth. We further demonstrate that sildenafil, when combined with statins, improves survival across multiple cancers, underscoring the importance of identifying the potential effects of existing drugs on carcinogenesis and highlighting the therapeutic potential of repurposing these drugs when beneficial for cancer treatment.

This observational study has several limitations. First, PDE5A inhibitor use was identified from EMR data, potentially missing patients obtaining treatment privately or online, leading to exposure misclassification. Second, confounding by indication may exist despite careful matching of exposed and non-exposed patients on clinical and

demographic variables. Third, the retrospective design does not allow causal inference in human patients, even though exposure preceded the outcome and causality was supported in mouse models. Finally, missing information on cancer stage and treatment constitutes an important unmeasured confounder that warrants further investigation.

Importantly, experiments using 4T1 triple-negative breast cancer and MC38 colon cancer models were performed in female mice, excluding conventional male-specific effects of PDE5A inhibitors. Moreover, our findings highlight the potential of PDE5A inhibitors as adjuvant therapies for these aggressive cancers that currently lack effective treatment options. Notably, sildenafil may also enhance chemotherapy delivery through its well-established vasodilatory effects on blood vessels. Beyond oncology, these findings suggest broader relevance to cardiovascular and neurodegenerative diseases linked to abnormal cholesterol trafficking(73),(74).

Acknowledgments

We greatly appreciate the valuable comments and suggestions from Monther Abu-Remaileh. We thank Yifat Merbl for her intellectual input and Assaf Kacen, Elena Ainbinder, Uwe Heinig, Angel Porgador, Roni Oren, Liat Alyagor, Shira Cohen, Philipp Selenko, and Yoseph Addadi for their technical guidance. We thank Yongmei Zhao for her assistance with depositing the RNA-Seq data into the GEO database. We thank Shira Albeck for her help in producing the D4-EGFP probe. The D4-EGFP plasmid was a kind gift from Fabien ALPY. The green cGULL plasmid was a kind gift from Prof. Yoav Shaul. A.E. is supported by research grants from Minerva, Israel Ministry of Health (3-18791), the Israel Science Foundation (873/23), and the Israel Cancer Research Fund (837124), the MAVRI (2335/25), and the Mark Endeavor Foundation. A.E is the Dean of the Miriam and Aaron Gutwirth Medical School and the Head of the David and Fela Shapell Family Center for Genetic Disorders Research. She is the incumbent of the Sir Ernst B. Chain Professorial Chair. The Moross Integrated Cancer Center, the EKARD Institute for Cancer Diagnosis Research, the Abisch-Frenkel RNA Therapeutics Center, Dr. Gilbert S. Omenn and Martha A. Darling, and the Koret Foundation generously supported the research conducted by AE's lab. Y.A is supported by the Dwek Institute for Cancer Therapy Research and the V. Levmore Tannor & S. Esses families. Optical images were acquired at the de

Picciotto Cancer Cell Observatory in memory of Wolfgang and Ruth Lesser of the Moross Integrated Cancer Center in the Department of Life Science Core Facilities, Weizmann Institute of Science. We acknowledge the use of artificial intelligence–based tools (Grammarly and ChatGPT) for English language editing and improvement of manuscript readability. The summary figure was created by the Weizmann graphic department (Itai Rave). The work of S.M and M.I was supported by the Vera and John Schwartz Family Center for Metabolic Biology.

References

1. Rabinovich S, Adler L, Yizhak K, Sarver A, Silberman A, Agron S*, et al.* Diversion of aspartate in ASS1-deficient tumours fosters de novo pyrimidine synthesis. Nature **2015**;527:379-83
2. Keshet R, Erez A. Arginine and the metabolic regulation of nitric oxide synthesis in cancer. Dis Model Mech **2018**;11
3. Keshet R, Lee JS, Adler L, Iraqi M, Ariav Y, Lim LQJ*, et al.* Targeting purine synthesis in ASS1-expressing tumors enhances the response to immune checkpoint inhibitors. Nat Cancer **2020**;1:894-908
4. Stehle D, Barresi M, Schulz J, Feil R. Heterogeneity of cGMP signalling in tumour cells and the tumour microenvironment: Challenges and chances for cancer pharmacology and therapeutics. Pharmacol Ther **2023**;242:108337
5. Buckley MS, Staib RL, Wicks LM, Feldman JP. Phosphodiesterase-5 inhibitors in management of pulmonary hypertension: safety, tolerability, and efficacy. Drug Healthc Patient Saf **2010**;2:151-61
6. Francis SH, Blount MA, Corbin JD. Mammalian cyclic nucleotide phosphodiesterases: molecular mechanisms and physiological functions. Physiol Rev **2011**;91:651-90
7. Dunkerly-Eyring B, Kass DA. Myocardial Phosphodiesterases and Their Role in cGMP Regulation. J Cardiovasc Pharmacol **2020**;75:483-93
8. Huang W, Sundquist J, Sundquist K, Ji J. Phosphodiesterase-5 inhibitors use and risk for mortality and metastases among male patients with colorectal cancer. Nat Commun **2020**;11:3191
9. Feil R, Kemp-Harper B. cGMP signalling: from bench to bedside. Conference on cGMP generators, effectors and therapeutic implications. EMBO Rep **2006**;7:149-53
10. Moskovits N, Peretz I, Chausky E, Itzhaki E, Shmuel N, Meerson R*, et al.* Palbociclib in combination with sunitinib exerts a synergistic anti-cancer effect in patient-derived xenograft models of various human cancers types. Cancer Lett **2022**;536:215665
11. Malitsky S, Ziv C, Rosenwasser S, Zheng S, Schatz D, Porat Z*, et al.* Viral infection of the marine alga Emiliania huxleyi triggers lipidome remodeling and induces the production of highly saturated triacylglycerol. New Phytol **2016**;210:88-96
12. Gnainsky Y, Itkin M, Mehlman T, Brandis A, Malitsky S, Soen Y. Protocol for studying microbiome impact on host energy and reproduction in Drosophila. STAR Protoc **2022**;3:101253
13. Ma L, Ouyang Q, Werthmann GC, Thompson HM, Morrow EM. Live-cell Microscopy and Fluorescence-based Measurement of Luminal pH in Intracellular Organelles. Front Cell Dev Biol **2017**;5:71

14. Wilhelm LP, Voilquin L, Kobayashi T, Tomasetto C, Alpy F. Intracellular and Plasma Membrane Cholesterol Labeling and Quantification Using Filipin and GFP-D4. Methods Mol Biol **2019**;1949:137-52
15. Barutcu AR, Lajoie BR, McCord RP, Tye CE, Hong D, Messier TL*, et al.* Chromatin interaction analysis reveals changes in small chromosome and telomere clustering between epithelial and breast cancer cells. Genome Biol **2015**;16:214
16. Robinson JL, Kocabas P, Wang H, Cholley PE, Cook D, Nilsson A*, et al.* An atlas of human metabolism. Sci Signal **2020**;13
17. Arafeh R, Shibue T, Dempster JM, Hahn WC, Vazquez F. The present and future of the Cancer Dependency Map. Nat Rev Cancer **2025**;25:59-73
18. Zur H, Ruppin E, Shlomi T. iMAT: an integrative metabolic analysis tool. Bioinformatics **2010**;26:3140-2
19. Orth JD, Thiele I, Palsson BO. What is flux balance analysis? Nat Biotechnol **2010**;28:245-8
20. Kwon HJ, Abi-Mosleh L, Wang ML, Deisenhofer J, Goldstein JL, Brown MS*, et al.* Structure of N-terminal domain of NPC1 reveals distinct subdomains for binding and transfer of cholesterol. Cell **2009**;137:1213-24
21. Lu C, Wu C, Ghoreishi D, Chen W, Wang L, Damm W*, et al.* OPLS4: Improving Force Field Accuracy on Challenging Regimes of Chemical Space. J Chem Theory Comput **2021**;17:4291-300
22. Sherman W, Day T, Jacobson MP, Friesner RA, Farid R. Novel procedure for modeling ligand/receptor induced fit effects. J Med Chem **2006**;49:534-53
23. Friesner RA, Banks JL, Murphy RB, Halgren TA, Klicic JJ, Mainz DT*, et al.* Glide: a new approach for rapid, accurate docking and scoring. 1. Method and assessment of docking accuracy. J Med Chem **2004**;47:1739-49
24. Halgren TA, Murphy RB, Friesner RA, Beard HS, Frye LL, Pollard WT*, et al.* Glide: a new approach for rapid, accurate docking and scoring. 2. Enrichment factors in database screening. J Med Chem **2004**;47:1750-9
25. Dagan N, Barda N, Kepten E, Miron O, Perchik S, Katz MA*, et al.* BNT162b2 mRNA Covid-19 Vaccine in a Nationwide Mass Vaccination Setting. N Engl J Med **2021**;384:1412-23
26. Rennert G, Rennert HS, Miron E, Peterburg Y. Population colorectal cancer screening with fecal occult blood test. Cancer Epidemiol Biomarkers Prev **2001**;10:1165-8
27. Krivoy A, Balicer RD, Feldman B, Hoshen M, Zalsman G, Weizman A*, et al.* Adherence to antidepressants is associated with lower mortality: a 4-year population-based cohort study. J Clin Psychiatry **2016**;77:e566-72
28. Glenn JR, Dovlatova N, White AE, Dhillon K, Heptinstall S, Fox SC. 'VASPFix' for measurement of VASP phosphorylation in platelets and for monitoring effects of P2Y12 antagonists. Thromb Haemost **2014**;111:539-48
29. Yang S, Zhang JJ, Huang XY. Mouse models for tumor metastasis. Methods Mol Biol **2012**;928:221-8
30. Guazzi M, Samaja M. The role of PDE5-inhibitors in cardiopulmonary disorders: from basic evidence to clinical development. Curr Med Chem **2007**;14:2181-91
31. Goldman O, Adler LN, Hajaj E, Croese T, Darzi N, Galai S*, et al.* Early infiltration of innate immune cells to the liver depletes HNF4a and promotes extra-hepatic carcinogenesis. Cancer Discov **2023**
32. Kuan YC, Takahashi Y, Maruyama T, Shimizu M, Yamauchi Y, Sato R. Ring finger protein 5 activates sterol regulatory element-binding protein 2 (SREBP2) to promote cholesterol biosynthesis via inducing polyubiquitination of SREBP chaperone SCAP. J Biol Chem **2020**;295:3918-28

33. Olzmann JA, Carvalho P. Dynamics and functions of lipid droplets. Nat Rev Mol Cell Biol **2019**;20:137-55
34. Maier CR, Hartmann O, Prieto-Garcia C, Al-Shami KM, Schlicker L, Vogel FCE*, et al.* USP28 controls SREBP2 and the mevalonate pathway to drive tumour growth in squamous cancer. Cell Death Differ **2023**;30:1710-25
35. Li X, Wu JB, Li Q, Shigemura K, Chung LW, Huang WC. SREBP-2 promotes stem cell-like properties and metastasis by transcriptional activation of c-Myc in prostate cancer. Oncotarget **2016**;7:12869-84
36. Tobert JA. Lovastatin and beyond: the history of the HMG-CoA reductase inhibitors. Nat Rev Drug Discov **2003**;2:517-26
37. Wu CC, Ko FN, Kuo SC, Lee FY, Teng CM. YC-1 inhibited human platelet aggregation through NO-independent activation of soluble guanylate cyclase. Br J Pharmacol **1995**;116:1973-8
38. Ishitsuka R, Saito T, Osada H, Ohno-Iwashita Y, Kobayashi T. Fluorescence image screening for chemical compounds modifying cholesterol metabolism and distribution. J Lipid Res **2011**;52:2084-94
39. Bairos JA, Njoku U, Zafar M, Akl MG, Li L, Parlakgul G*, et al.* Sterol O-acyltransferase (SOAT/ACAT) activity is required to form cholesterol crystals in hepatocyte lipid droplets. Biochim Biophys Acta Mol Cell Biol Lipids **2024**;1869:159512
40. Paukner K, Kralova Lesna I, Poledne R. Cholesterol in the Cell Membrane-An Emerging Player in Atherogenesis. Int J Mol Sci **2022**;23
41. Kenworthy AK, Schmieder SS, Raghunathan K, Tiwari A, Wang T, Kelly CV*, et al.* Cholera Toxin as a Probe for Membrane Biology. Toxins (Basel) **2021**;13
42. Motoyama K, Kameyama K, Onodera R, Araki N, Hirayama F, Uekama K*, et al.* Involvement of PI3K-Akt-Bad pathway in apoptosis induced by 2,6-di-O-methyl-beta-cyclodextrin, not 2,6-di-O-methyl-alpha-cyclodextrin, through cholesterol depletion from lipid rafts on plasma membranes in cells. Eur J Pharm Sci **2009**;38:249-61
43. Biswas A, Kashyap P, Datta S, Sengupta T, Sinha B. Cholesterol Depletion by MbetaCD Enhances Cell Membrane Tension and Its Variations-Reducing Integrity. Biophys J **2019**;116:1456-68
44. Yu W, Gong JS, Ko M, Garver WS, Yanagisawa K, Michikawa M. Altered cholesterol metabolism in Niemann-Pick type C1 mouse brains affects mitochondrial function. J Biol Chem **2005**;280:11731-9
45. Brand MD, Nicholls DG. Assessing mitochondrial dysfunction in cells. The Biochemical journal **2011**;435:297-312
46. Grabner GF, Fawzy N, Pribasnig MA, Trieb M, Taschler U, Holzer M*, et al.* Metabolic disease and ABHD6 alter the circulating bis(monoacylglycerol)phosphate profile in mice and humans. J Lipid Res **2019**;60:1020-31
47. Platt FM, d'Azzo A, Davidson BL, Neufeld EF, Tifft CJ. Lysosomal storage diseases. Nat Rev Dis Primers **2018**;4:27
48. Skeyni A, Pradignac A, Matz RL, Terrand J, Boucher P. Cholesterol trafficking, lysosomal function, and atherosclerosis. Am J Physiol Cell Physiol **2024**;326:C473-C86
49. Wang WA, Agellon LB, Michalak M. Endoplasmic reticulum calcium dictates the distribution of intracellular unesterified cholesterol. Cell Calcium **2018**;76:116-21
50. Lukowski R, Feil R. Recent developments in cGMP research: From mechanisms to medicines and back. Br J Pharmacol **2022**;179:2321-7
51. Festa BP, Chen Z, Berquez M, Debaix H, Tokonami N, Prange JA*, et al.* Impaired autophagy bridges lysosomal storage disease and epithelial dysfunction in the kidney. Nat Commun **2018**;9:161
52. Patterson M. Niemann-Pick Disease Type C. In: Adam MP, Feldman J, Mirzaa GM, Pagon RA, Wallace SE, Bean LJH*, et al.*, editors. GeneReviews((R)). Seattle (WA)1993.

53. Colombo A, Dinkel L, Muller SA, Sebastian Monasor L, Schifferer M, Cantuti-Castelvetri L*, et al.* Loss of NPC1 enhances phagocytic uptake and impairs lipid trafficking in microglia. Nat Commun **2021**;12:1158
54. Fazliyeva R, Makhov P, Uzzo RG, Kolenko VM. Targeting NPC1 in Renal Cell Carcinoma. Cancers (Basel) **2024**;16
55. Lu F, Liang Q, Abi-Mosleh L, Das A, De Brabander JK, Goldstein JL*, et al.* Identification of NPC1 as the target of U18666A, an inhibitor of lysosomal cholesterol export and Ebola infection. Elife **2015**;4
56. Prabhu AV, Kang I, De Pace R, Wassif CA, Fujiwara H, Kell P*, et al.* A human iPSC-derived inducible neuronal model of Niemann-Pick disease, type C1. BMC Biol **2021**;19:218
57. Albrecht LV, Tejeda-Munoz N, De Robertis EM. Protocol for Probing Regulated Lysosomal Activity and Function in Living Cells. STAR Protoc **2020**;1:100132
58. Han S, Wang Q, Song Y, Pang M, Ren C, Wang J*, et al.* Lithium ameliorates Niemann-Pick C1 disease phenotypes by impeding STING/SREBP2 activation. iScience **2023**;26:106613
59. Lee JS, Nair NU, Dinstag G, Chapman L, Chung Y, Wang K*, et al.* Synthetic lethality-mediated precision oncology via the tumor transcriptome. Cell **2021**;184:2487-502 e13
60. Kukreja RC, Salloum FN, Das A. Cyclic guanosine monophosphate signaling and phosphodiesterase-5 inhibitors in cardioprotection. J Am Coll Cardiol **2012**;59:1921-7
61. Xie X, Brown MS, Shelton JM, Richardson JA, Goldstein JL, Liang G. Amino acid substitution in NPC1 that abolishes cholesterol binding reproduces phenotype of complete NPC1 deficiency in mice. Proc Natl Acad Sci U S A **2011**;108:15330-5
62. Wei JY, Cohen ED, Genieser HG, Barnstable CJ. Substituted cGMP analogs can act as selective agonists of the rod photoreceptor cGMP-gated cation channel. J Mol Neurosci **1998**;10:53-64
63. Jiang SY, Li H, Tang JJ, Wang J, Luo J, Liu B*, et al.* Discovery of a potent HMG-CoA reductase degrader that eliminates statin-induced reductase accumulation and lowers cholesterol. Nat Commun **2018**;9:5138
64. Riscal R, Bull CJ, Mesaros C, Finan JM, Carens M, Ho ES*, et al.* Cholesterol Auxotrophy as a Targetable Vulnerability in Clear Cell Renal Cell Carcinoma. Cancer Discov **2021**;11:3106-25
65. Barbalata CI, Tefas LR, Achim M, Tomuta I, Porfire AS. Statins in risk-reduction and treatment of cancer. World J Clin Oncol **2020**;11:573-88
66. Tzoumas N, Farrah TE, Dhaun N, Webb DJ. Established and emerging therapeutic uses of PDE type 5 inhibitors in cardiovascular disease. Br J Pharmacol **2020**;177:5467-88
67. Zhang Z, Huang W, Huang D, Xu Z, Xie Q, Tan X*, et al.* Repurposing of phosphodiesterase-5 inhibitor sildenafil as a therapeutic agent to prevent gastric cancer growth through suppressing c-MYC stability for IL-6 transcription. Commun Biol **2025**;8:85
68. Weed DT, Vella JL, Reis IM, De la Fuente AC, Gomez C, Sargi Z*, et al.* Tadalafil reduces myeloid-derived suppressor cells and regulatory T cells and promotes tumor immunity in patients with head and neck squamous cell carcinoma. Clin Cancer Res **2015**;21:39-48
69. Catalano S, Campana A, Giordano C, Gyorffy B, Tarallo R, Rinaldi A*, et al.* Expression and Function of Phosphodiesterase Type 5 in Human Breast Cancer Cell Lines and Tissues: Implications for Targeted Therapy. Clin Cancer Res **2016**;22:2271-82
70. Klutzny S, Anurin A, Nicke B, Regan JL, Lange M, Schulze L*, et al.* PDE5 inhibition eliminates cancer stem cells via induction of PKA signaling. Cell Death Dis **2018**;9:192

71. Hryniewicz-Jankowska A, Augoff K, Sikorski AF. The role of cholesterol and cholesterol-driven membrane raft domains in prostate cancer. Exp Biol Med (Maywood) **2019**;244:1053-61
72. Fernandez LP, Gomez de Cedron M, Ramirez de Molina A. Alterations of Lipid Metabolism in Cancer: Implications in Prognosis and Treatment. Front Oncol **2020**;10:577420
73. Fang J, Zhang P, Zhou Y, Chiang CW, Tan J, Hou Y*, et al.* Endophenotype-based in silico network medicine discovery combined with insurance record data mining identifies sildenafil as a candidate drug for Alzheimer's disease. Nat Aging **2021**;1:1175-88
74. O'Hagan R, Berg AR, Hong CG, Parel PM, Mehta NN, Teague HL. Systemic consequences of abnormal cholesterol handling: Interdependent pathways of inflammation and dyslipidemia. Front Immunol **2022**;13:972140

Figure Legends:

Figure 1 – Sildenafil restricts cancer progression. **A.** Western blot analysis of Phospho Vasodilator Stimulated Phosphoprotein (phospho-VASP) (Ser239) and Glyceraldehyde 3-phosphate dehydrogenase (GAPDH) in 4T1, LLC, and MC38 cells treated with 100 μM sildenafil for the indicated time points. Lower panels show Image quantification of relative pVASP expression. **B.** Plasma Cyclic guanosine monophosphate (cGMP) quantification in sildenafil-treated BALB/c and C57BL/6 mice. BALB/c: control N=6, sildenafil N=7. C57BL/6: control N=5, sildenafil N=6. **C.** Cell viability measured by crystal violet following 24 h sildenafil treatment. N=3/group. **D-E**- 4T1 (**Upper panel**), LLC (**Middle panel**), and MC38 (**Lower panel**). **D.** Cell migration quantified by IncuCyte live-cell imaging after sildenafil treatment. Wound confluence was monitored for 24–48 h. Scale bars, 200 μm. **E.** Representative lung H&E staining and metastatic burden quantification following intravenous tumor injection and sildenafil treatment. **F.** Spontaneous breast metastasis model using 4T1 cells injected into BALB/c mice followed by sildenafil treatment. **G.** In silico genome-scale metabolic modeling comparing proliferation and migration fluxes in DepMap cancerous and noncancerous cell lines with or without sildenafil. Sildenafil selectively reduced migration flux in cancer cells. **H.** Kaplan–Meier survival curves of lung and colon cancer patients treated with sildenafil. Data are presented as mean ± SD. Unless otherwise indicated, statistical analyses were performed using two-tailed Student's t-tests. For all panels *$p \leq 0.05$; **$p \leq 0.005$; ***$p \leq 0.0005$; ****$p \leq 0.00005$.

Figure 2 – Sildenafil treatment gives rise to cholesterol biosynthesis and alters cellular and organelle membranes. A. Gene Set Enrichment Analysis (GSEA) of RNA-seq data from 4T1 cells treated with sildenafil for 24 h. **B**. Immunofluorescence analysis of sterol regulatory element–binding protein 2 (SREBP2) (green) and DRAQ5 (red) nuclear localization following sildenafil treatment. Right panel shows Cytation10 quantification (N=6). **C.** Western blot and Image quantification of cholesterol synthesis-related proteins (Mevalonate Kinase (MVK), 3-hydroxy-3-methylglutaryl-CoA synthase 1 (HMGCS1), Lanosterol Synthase (LSS), and LDL receptor (LDLR)) following sildenafil treatment. **D.** Gas chromatography/mass spectrometry (GC/MS) quantification of free and esterified cholesterol in 4T1 cells treated with lovastatin or sildenafil for 24 h (N=4/group). **E.** Cholesterol quantification in triple-Negative Breast Cancer (TNBC) patient-derived cells (383B, 283, 152C) treated with sildenafil for 24 h using the Cholesterol/Cholesterol Ester-Glo™ assay. **F.** Western blot analysis of pVASP levels in sildenafil-, YC-1–treated, or shPDE5a-expressing 4T1 cells. Right panel shows Image quantification. **G.** Representative immunofluorescence images of 4T1 cells stained with BODIPY (green) , Filipin (yellow) , and DRAQ5 (magenta) after sildenafil treatment. Right panel shows Filipin/BODIPY co-localization quantification (N=3). Scale bars, 10 μm. **H.** Lipid droplet and lysosome accumulation following sildenafil or YC-1 treatment visualized using BODIPY (green), LysoTracker (red) and Hoesct (blue) for DNA staining. Scale bars, 20 μm. **I.** Volcano plots from lipidomics analysis of sildenafil-treated 4T1 cells showing increased triglycerides (TG) and decreased phosphatidylcholines (PC) (N=4/group). **J.** Lipid raft analysis using Cholera toxin subunit B (CTSB-far red) and with Hoechst (blue) for DNA staining following sildenafil and cholesterol treatments. Quantification was performed using Gen5 software. Scale bars, 20 μm. **K.** Seahorse analysis of mitochondrial respiration in 4T1 cells treated with sildenafil. **L.** Migration analysis of 4T1 cells treated with sildenafil and/or water-soluble cholesterol using IncuCyte wound-confluence assays FOR QUANTIFICATION (Right panel). Scale bars, 200 μm. **M.** Immunofluorescence analysis of lipid droplets following sildenafil and cholesterol treatments using BODIPY (green) and Hoechst (blue) for DNA staining. Quantification was performed using Gen5 software (Right panel). Scale bars, 20 μm. Data are presented as mean ± SD. Unless otherwise indicated, statistical analyses were performed using two-tailed Student's t-tests. For all panels *$p \leq 0.05$; **$p \leq 0.005$; ***$p \leq 0.0005$; ****$p \leq 0.00005$.

Figure 3 – Sildenafil induces cholesterol accumulation in lysosomes. A. Transmission electron microscopy demonstrating accumulation of autophagic vesicles and cholesterol aggregates following sildenafil treatment. Right panel shows quantification of autophagic vesicles per cell. **B.** Representative images of 4T1 cells stained with LysoTracker, BODIPY, and Hoechst following sildenafil treatment. Right panel shows Gen5 quantification of lysosomes, lipid droplets, and co-localization (N=3/group). Scale bars, 20 μm. **C.** Filipin and LAMP1 co-localization analysis in sildenafil-treated 4T1 cells. Right panel shows ImageJ quantification (N=5/group). Scale bars, 10 μm. **D.** Western blot analysis of autophagy markers LC3B and P62 in sildenafil-treated 4T1 cells. Right panel shows Image quantification. **E.** Immunofluorescence analysis of LC3B puncta following sildenafil treatment. Quantification was performed using Gen5 software (N=6/group). Scale bars, 20 μm. **F.** Immunofluorescence analysis of P62 puncta following sildenafil treatment. Quantification was performed using Gen5 software (N=5/group). Scale bars, 20 μm. **G.** Western blot analysis of LC3B and P62 in 4T1 cells treated with sildenafil, bafilomycin A1, or both. Right panel shows Image quantification. Data are presented as mean ± SD. Unless otherwise indicated, statistical analyses were performed using two-tailed Student's t-tests. For all panels *p≤0.05; **p≤0.005; ***p≤0.0005; ****p≤0.00005.

Figure 4- Downregulating NPC1 recapitulates sildenafil-treated cancer-restricting phenotype. A. qPCR analysis of NPC1 and NPC2 expression in shNPC1- or shGFP-expressing 4T1 cells. **B.** Western blot analysis and Image quantification of NPC1 and NPC2 protein levels in shNPC1 and control cells. **C.** Filipin staining of cholesterol accumulation in shNPC1 or sildenafil/U18666A-treated 4T1 cells. Scale bars, 20 μm. **D.** Lysosomal pH quantification using LysoSensor following sildenafil or U18666A treatment (N=5/group). **E.** qPCR analysis of cholesterol-related genes in shNPC1 and control 4T1 cells. **F.** Western blot analysis and quantification of cholesterol synthesis proteins (LSS, HMGCS1, MVK) in shNPC1 cells. **G.** Colony formation assays of shNPC1 and control 4T1 cells treated with sildenafil. Quantification was performed using ImageJ software. **H.** H&E staining and metastatic burden quantification of lungs from mice injected with shNPC1 or control 4T1 cells (N=6/group). **I**. IncuCyte proliferation analysis of shNPC1 and control 4T1 cells treated

with sildenafil. **J.** IncuCyte migration analysis of shNPC1 and control 4T1 cells treated with sildenafil. **K.** Molecular dynamics simulations showing RMSD values of NPC1 interactions with cGMP, cholesterol, and 8-pCPT-cGMP over 500 ns. **L.** qPCR analysis of cholesterol-related genes in 4T1 cells treated with sildenafil or 8-pCPT-cGMP. **M.** Filipin staining of cholesterol accumulation following sildenafil or 8-pCPT-cGMP treatment. Scale bars, 20 μm. **N.** Surface plasmon resonance (SPR) analysis demonstrating cGMP binding to NPC1 protein. Data are presented as mean ± SD. Unless otherwise indicated, statistical analyses were performed using two-tailed Student's t-tests. . For all panels *p≤0.05; **p≤0.005; ***p≤0.0005; ****p≤0.00005.

Figure 5 – Cancer cells express low levels of lysosomal genes and a higher sensitivity to sildenafil. A. Schematic overview of the analysis pipeline comparing RNA-seq profiles of sildenafil-sensitive and resistant cancer cell lines with non-cancerous controls using CTD2 and DESeq2 analyses. **B.** GO enrichment analysis showing significant downregulation of lysosomal and vacuolar transport pathways in sildenafil-sensitive cancer cell lines. **C.** Violin plots showing reduced lysosomal gene expression z-scores in predicted sildenafil-sensitive TCGA patient groups relative to normal and low-sensitive samples. **D.** Tumor-type stratified analysis of lysosomal gene expression across BRCA, COAD, and LUAD TCGA cohorts. **E.** Genome-scale metabolic modeling demonstrates reduced migration-associated fluxes following combined lysosomal transport knockout and sildenafil perturbation in cancer models. **F.** Analysis of publicly available datasets showing reduced lysosomal gene expression in MCF7 cells compared with nonmalignant MCF10A cells. **G.** qPCR validation of reduced LAMP1 and ARSB expression in MCF7 relative to MCF10A cells. **H.** Immunofluorescence analysis of LAMP1 expression in MCF7 cells expressing empty vector or LAMP1-overexpression constructs. Quantification was performed using Gen5 software. Scale bars, 20 μm. **I.** IncuCyte migration analysis of MCF7 cells expressing LAMP1-overexpression constructs and treated with sildenafil. Data are presented as mean ± SD. Unless otherwise indicated, statistical analyses were performed using two-tailed Student's t-tests. For all panels *p≤0.05; **p≤0.005; ***p≤0.0005; ****p≤0.00005.

Figure 6 – Sildenafil synergizes with cholesterol synthesis inhibition to increase cancer patients' survival. **A**. IncuCyte migration analysis of 4T1 cells treated with sildenafil, lovastatin, or both. Combination treatment produced the strongest inhibition of migration. **B**. Migration analysis of 4T1 cells cultured in lipid-depleted serum (LDPS) and treated with sildenafil. Combined cholesterol depletion and sildenafil significantly reduced migration. **C**. Flow cytometry analysis of apoptosis in 4T1 cells cultured with or without LDPS and treated with sildenafil for 48 h. **D.** Immunofluorescence analysis of plasma membrane cholesterol using D4-EGFP and Filipin staining following sildenafil and lovastatin treatment. Right panel shows quantification of filipin-positive cells and plasma membrane cholesterol levels. **E.** Tumor growth analysis of DU145 xenografts in nude mice treated with sildenafil, lovastatin, or both. Combination therapy significantly reduced tumor growth. **F.** H&E staining and quantification of lung metastases in 4T1-injected BALB/c mice treated with sildenafil, lovastatin, or both. Combination treatment showed the greatest reduction in metastatic burden. **G.** Kaplan–Meier survival analysis of male cancer patients from the Clalit database receiving sildenafil, statins, or combination treatment compared with untreated controls. **H.** Schematic model illustrating how sildenafil-induced cGMP signaling inhibits NPC1-mediated lysosomal cholesterol export, leading to lysosomal lipid accumulation, reduced cholesterol availability, membrane dysfunction, and suppression of metastasis. Combined statin treatment further enhances these anti-metastatic effects by blocking de novo cholesterol synthesis.

For panels A–G, data are presented as mean ± SD. Unless otherwise indicated, statistical analyses were performed using two-tailed Student's t-tests. For all panels *$p \leq 0.05$; **$p \leq 0.005$; ***$p \leq 0.0005$; ****$p \leq 0.00005$.

Figure 1

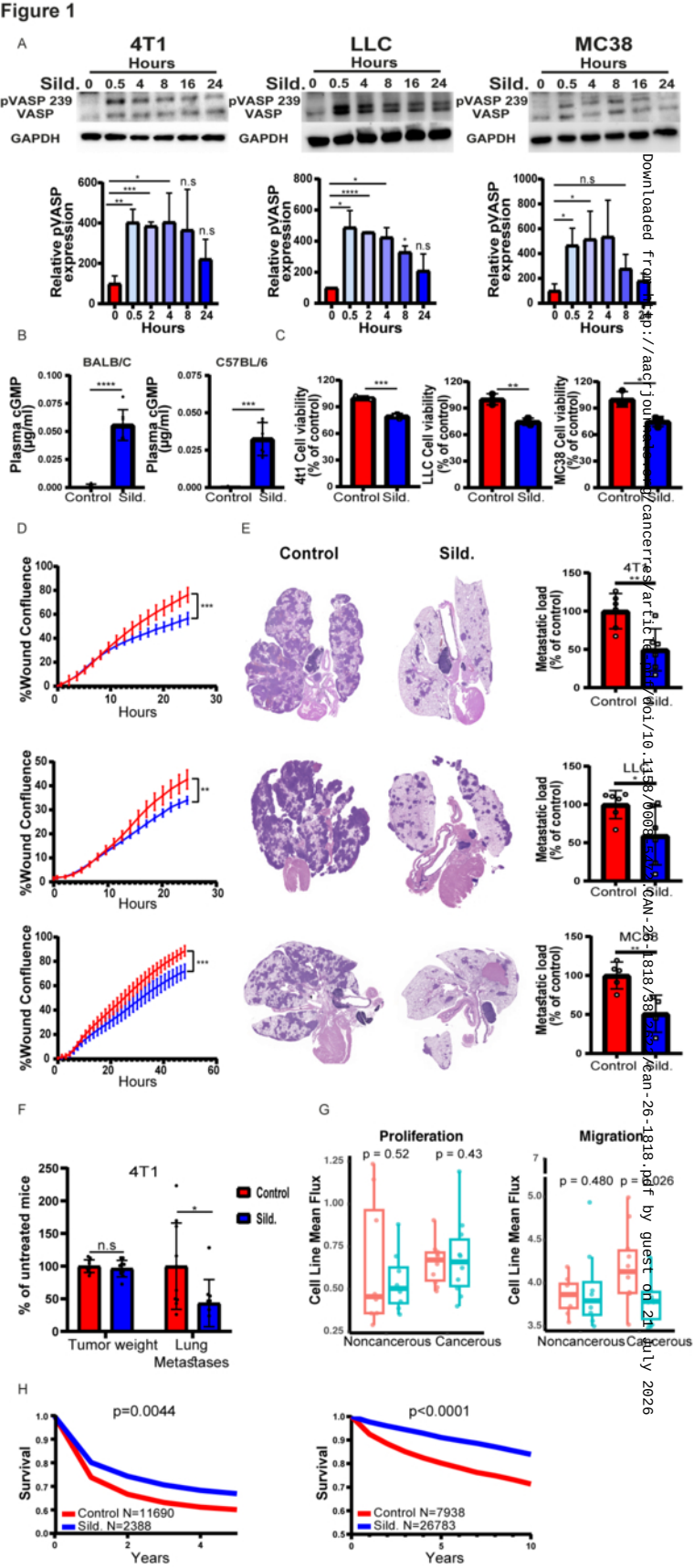

Figure 2

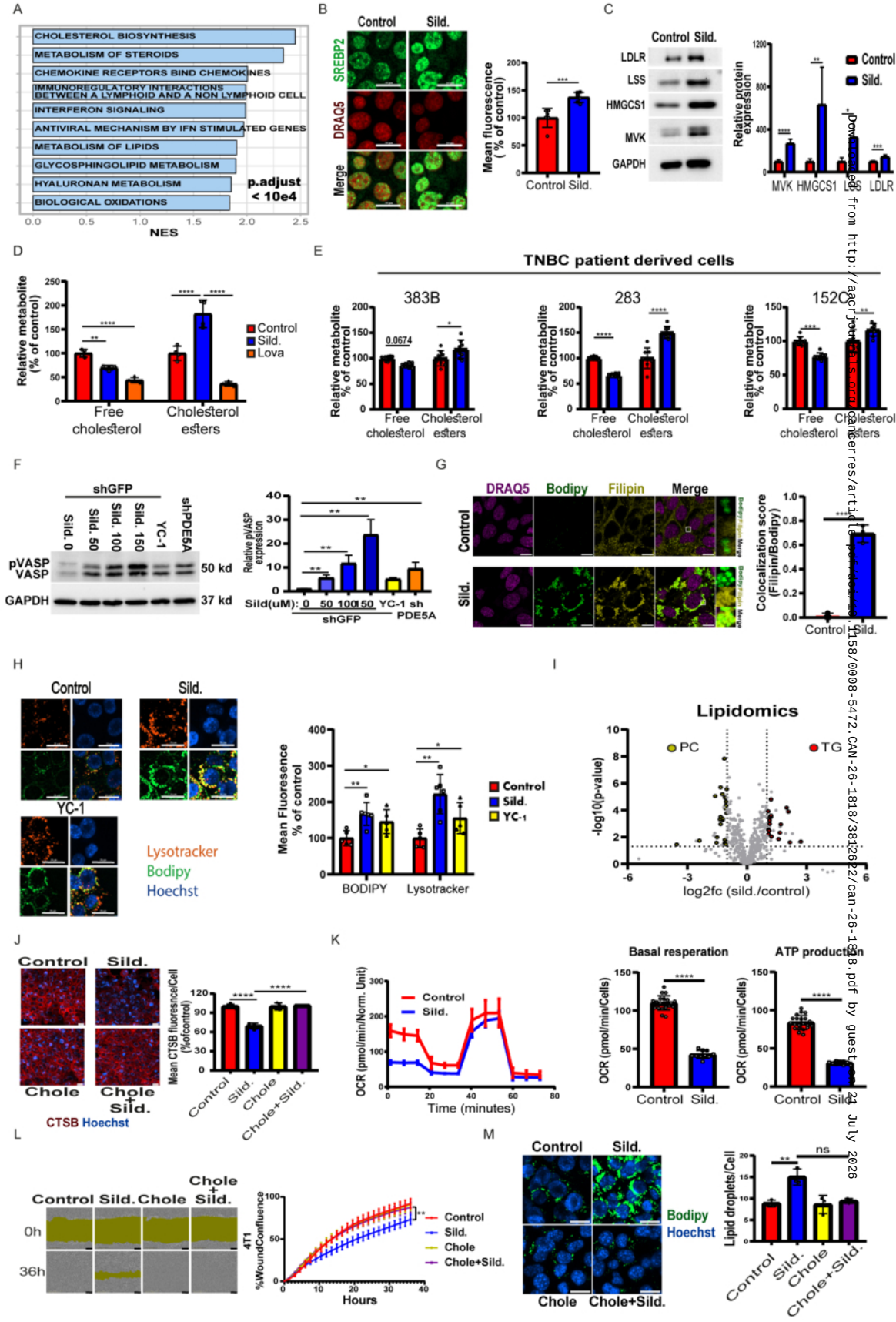

Figure 3

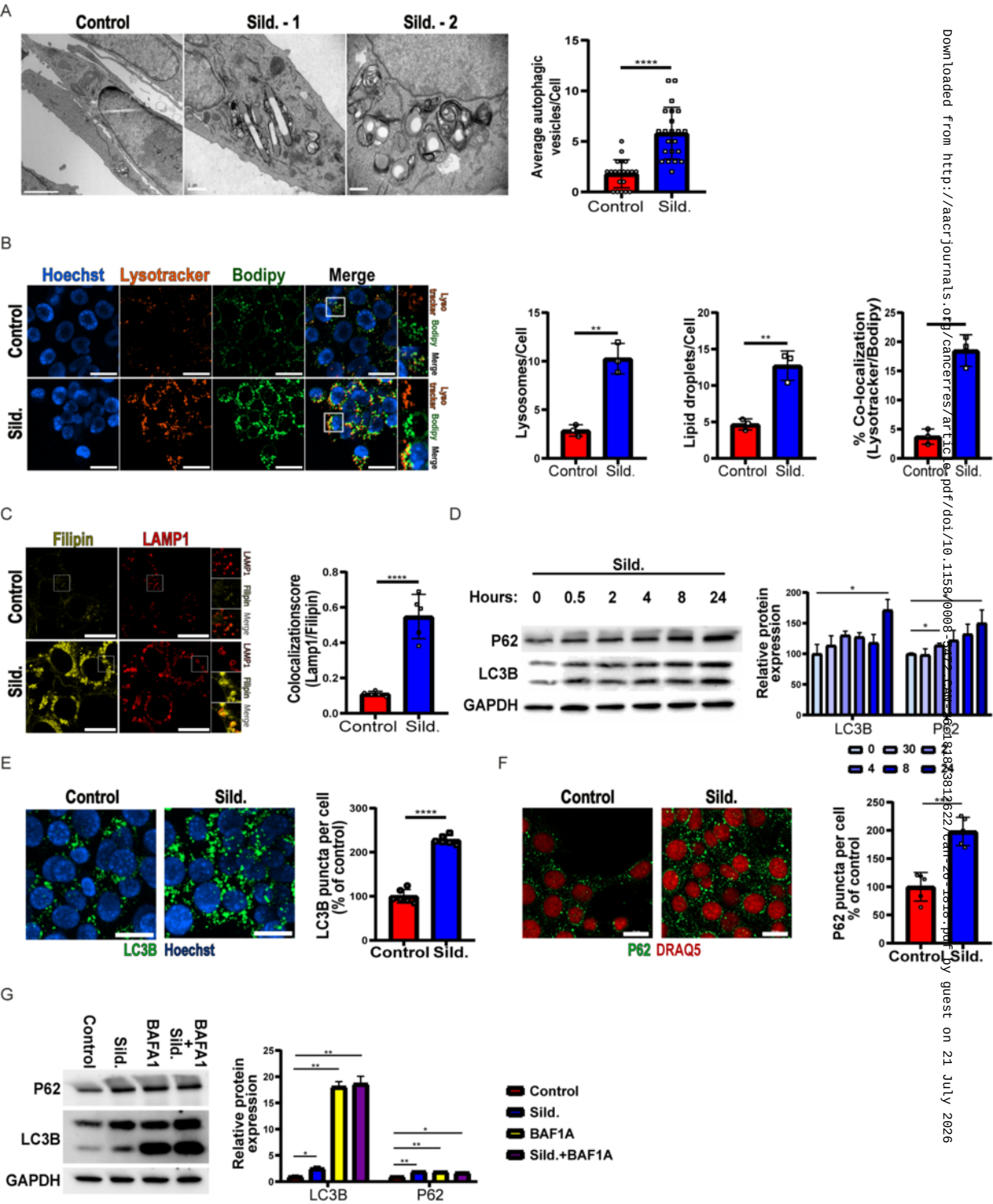

Figure 4

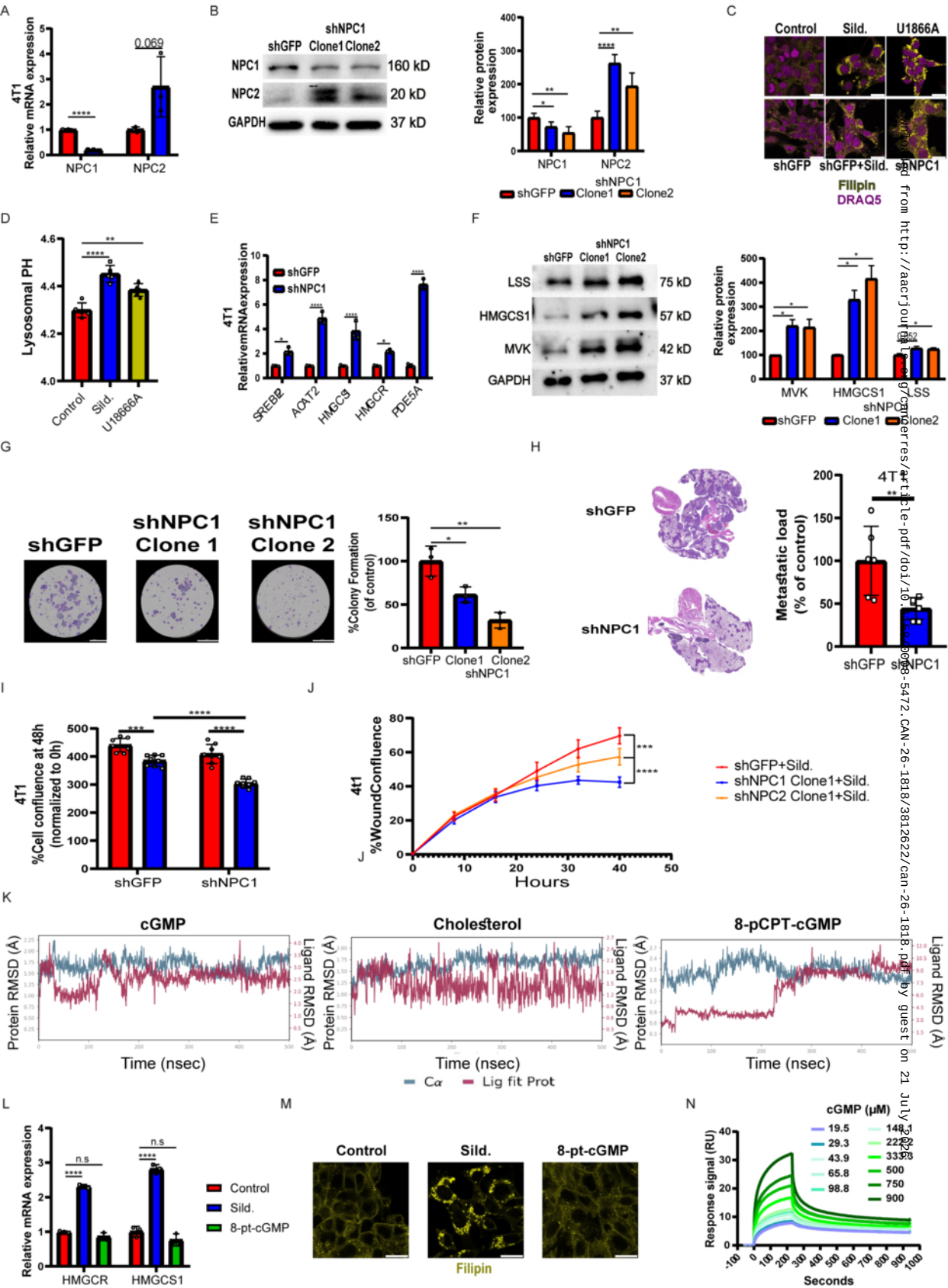

Figure 5

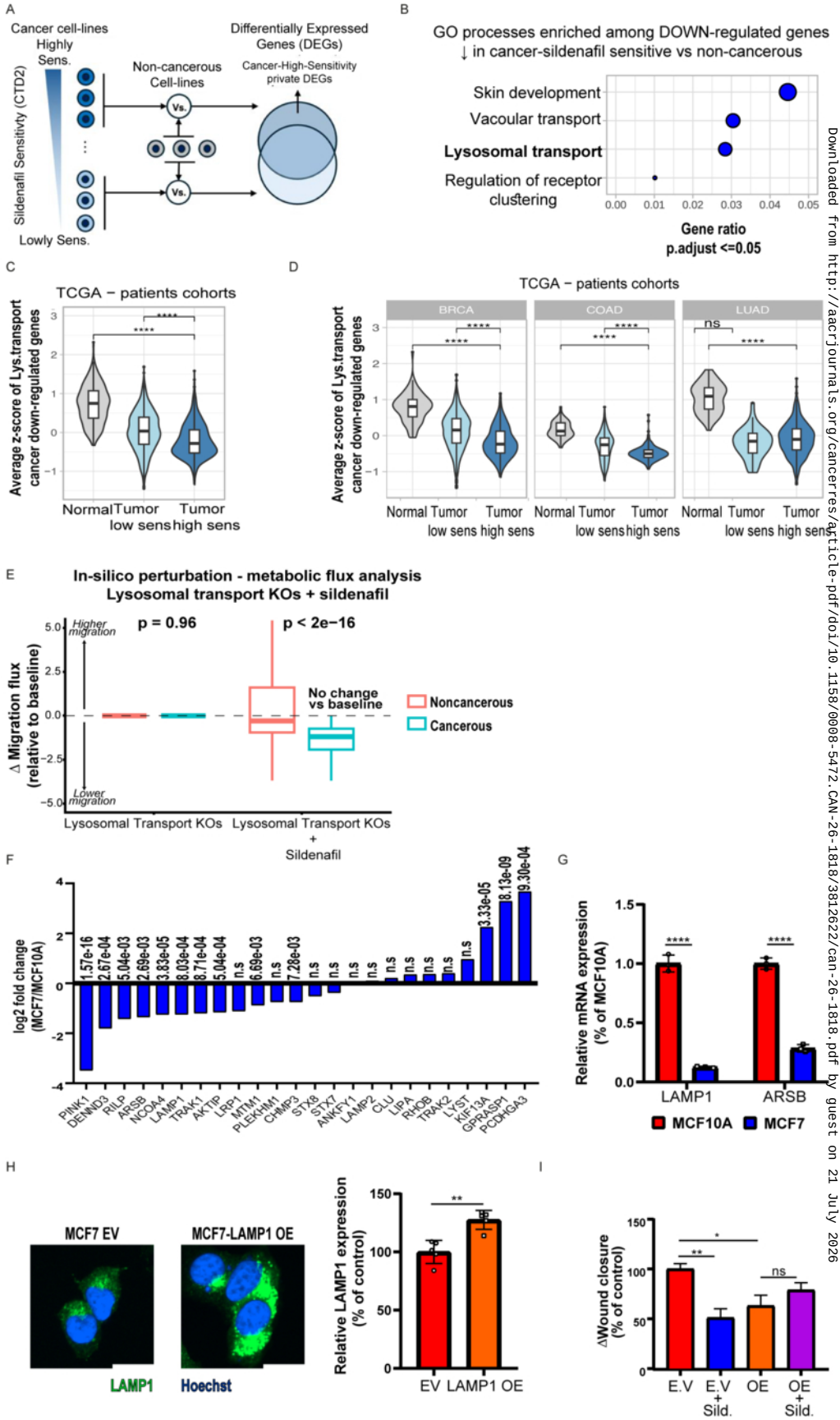

Figure 6